Contents — T through Z

INTERANNUAL COMPARISON OF WATER VAPOR IN THE NORTH POLAR REGION OF MARS. L. K. Tamppari[1], M. D. Smith[2], A. S. Hale[3], and D. S. Bass[3], [1]NASA Jet Propulsion Laboratory (4800 Oak Grove Drive, Pasadena, CA 91109 leslie.k.tamppari@jpl.nasa.gov), [2]NASA Goddard Space Flight Center (Michael.D.Smith.1@gsfc.nasa.gov), [3]NASA Jet Propulsion Laboratory (MS 264-235, 4800 Oak Grove Drive, Pasadena, CA 91109 amy.s.hale@jpl.nasa.gov), [4]NASA Jet Propulsion Laboratory (MS T1722, 4800 Oak Grove Drive, Pasadena, CA 91109 deborah.s.bass@jpl.nasa.gov).

Introduction: The Martian water cycle is one of the three annual cycles on Mars, dust and CO2 being the other two. Despite the fact that detailed spacecraft data, including global and annual coverage in a variety of wavelengths, have been taken of Mars spanning more than 25 years, there are many outstanding questions regarding the water cycle.

There is very little exposed water on Mars today, in either the atmosphere or on the surface [1] although there is geological evidence of catastrophic flooding and continuously running water in past epochs in Mars' history [2] as well as recent (within about 10,000 years ago) evidence for running water in the form of gullies [3].

The north polar cap region is of special interest as the residual cap is the main known reservoir of water on the planet today. The south polar residual cap may contain water, but presents a CO2 ice covering, even during southern summer. This hemispheric dichotomy is unexplained and is especially puzzling due to the fact that the Martian southern summer is much warmer (due to Mars' eccentricity) than the northern summer. Recently, water has been found in the top meter of the surface in both the northern and southern high latitude regions [e.g. 4-5] indicating an even greater amount of water on Mars than previously known.

Background: In order to better understand the current climate of Mars, we seek to understand atmospheric water in the north polar region. Our approach is to examine the water transport and cycling issues within the north polar region and in/out of the region on seasonal and annual timescales. Viking Mars Atmospheric Water Detector (MAWD) data showed that water vapor increased as the northern summer season progressed and temperatures increased, and that vapor appeared to be transported southward [6]. However, there has been uncertainty about the amount of water cycling in and out of the north polar region, as evidenced by residual polar cap visible brightness changes between one Martian year (Mariner 9 data) and a subsequent year (Viking data). These changes were originally thought to be interannual variations in the amount of frost sublimed based on global dust storm activity [5-7]. However, Viking thermal and imaging data were re-examined and it was found that 14-35 pr □m of water -ice appeared to be deposited on the cap later in the summer season [9], indicating that some water may be retained and redistributed within the polar cap region. This late summer deposition could be due to adsorption directly onto the cap surface or due to snowfall. We seek to understand what happens to the water on seasonal and interannual timescales. We address these issues by examining water vapor in the north polar region of Mars during the north spring and summer period from MGS TES data and by comparing these results to the Viking MAWD results.

Method:

Water vapor. Smith *et al.* [10] have performed retrievals for the column-integrated abundance of water vapor using the rotational water vapor bands at 220-360 cm^{-1}. Atmospheric temperatures are first retrieved using the 15-□m CO_2 band (Conrath *et al.*, 2000). Next, a forward radiative transfer computation is used to find the column-integrated water abundance that best fits the observed water vapor bands. At this time water is assumed to be well-mixed up to the condensation level and then zero above that. A total of six water vapor bands between 220 and 360 cm^{-1} are observed in TES spectra and the widths and relative depths of all six bands are very well fit by the synthetic spectra. Because the spectral signature of water vapor is spectrally very distinct from those of dust and water-ice, we can easily separate the relative contributions from each component (dust, water-ice, and water vapor) on a spectrum-by-spectrum basis.

Recent analysis with MGS TES data has shown evidence for water vapor "pulses" as the seasonal north polar cap sublimes [15]. This could be linked to the previous late-summer season deposition, discussed above. There appear to be significant differences in the details of the water vapor as a function of latitude and season between the Viking era and the current era (Figure 1). These differences may be a degree of interannual variability in the water vapor or a result of the coverage differences (Figure 2). Note that in Fig. 2, there are large differences in the MAWD coverage between the Ls=80°-95° bin (bin 7) vs. the Ls=95°-110° bin (bin 8). The TES coverage is much more uniform over time due to its orbit. An understanding of these possible interannual differences is important in several ways: (1) to understand the Martian climate, (2) to characterize the extent of interannual variability or lack thereof , and (3) to understand water-cycling within the north polar region and potentially in/out of the region. We will present our results of the investigation of the differences in these water vapor column amounts.

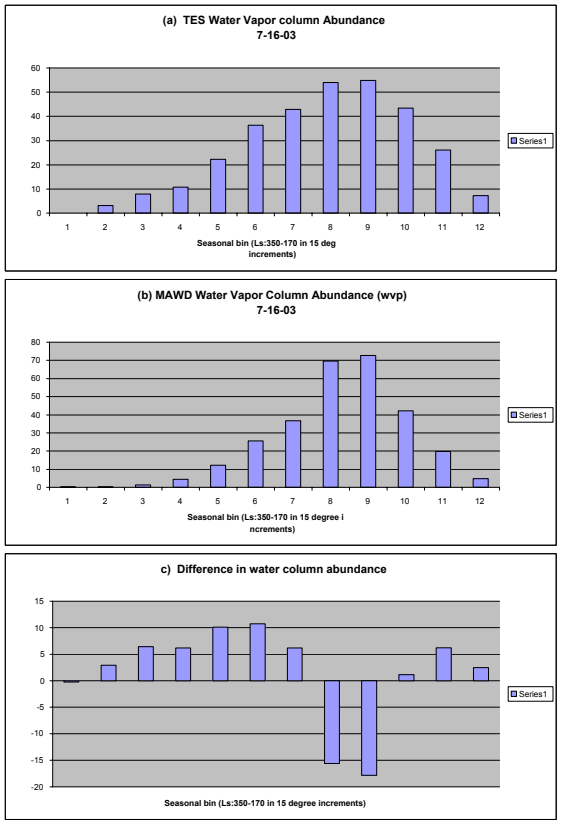

Figure 1. (a) TES water vapor column abundance in pr microns for the north polar region (60°-90°N). The seasonal binning is plotted Ls=15° increments, beginning at Ls=350° and ending at Ls=170°. Note that there is no TES data plotted for the first seasonal bin, Ls=350°-5°. (b) MAWD water vapor column abundance for same region and seasonal bins. MAWD data are shown for Ls=350°-5°. (c) The difference between the TES water vapor column abundance amount and the MAWD water vapor column abundance amount as a function of season.

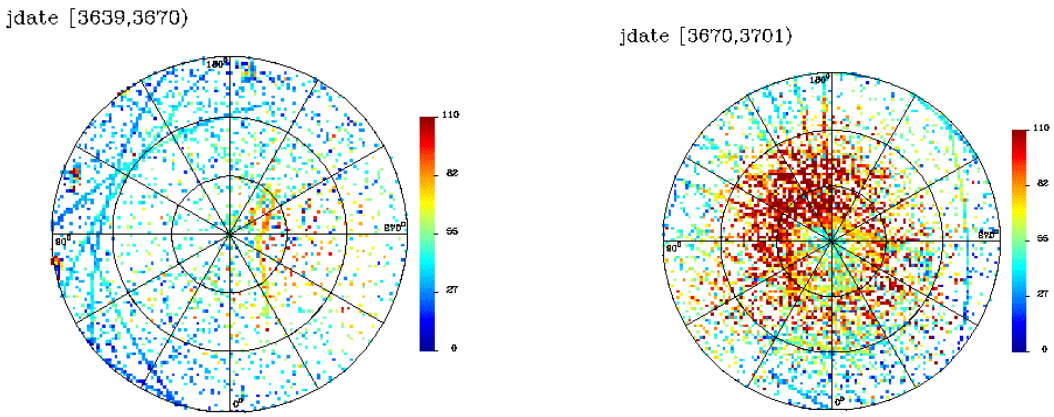

Figure 2. (Left) MAWD water vapor coverage shown for the Ls=80°-95° bin (bin 7). (Right) Similar for the Ls=95°-110° bin (bin 8). Note that the coverage near the cap center is much denser for the later season, possibly explaining the greater amount of water vapor measured during that season than in the previous season.

References: [1] Keiffer H. H. et al. (1976) *Science*, 194, 1341-1344 [2] Carr, M. H. (1998) *Water on Mars* [3] Malin M. C. and Edgett, K. S. (2001) *JGR* 106, 23429-23570. [8] Feldman W. C. et al., (2002) *Science* 297, 75-78 [4] Boynton W. V. et al., (2002) *Science* 297, 81-85 [5] Jakosky, B. M. (1985), Space Sci. Rev. 41, 131-200. [6] James P. B. and Martin L. (1985) *Bull. Amer. Astron. Soc., 17,* 735. [7] Kieffer H H. (1990) *JGR, 96,* 1481-1493. [8] Tamppari L. K. and Bass D. S. (2000) *2nd Mars Polar Conf.* [9] Tamppari L. K. et al. (2002) *Bull. 34th Am. Astron. Soc.,* 845. [10] Smith M. D. et al. (2000), *Bull. AAS*, 32(3), 1094.

THE SOUTH POLAR RESIDUAL CAP OF MARS:LAYERS, EROSION, AND STRATIGRAPHY. P. C. Thomas[1] [1]Center for Radiophysics and Space Research, Cornell University, Ithaca NY, 14853.

The south polar residual cap (sprc) of Mars is a group of thin layers degraded into unique topography resting on the flatter portions of the main polar layered deposits. This is a summary of the characteristics of these layers and their degredation that impacts the interpretation of the history of the martian polar environment..

Residual cap layers: There are two primary sets of depositional units in the sprc: 1) An older unit, approximately 10 m in thickness with four or five included layers, widely distributed over the sprc, and expressed as mesas or broad surfaces cut by a variety of circular to linear depressions, and commonly having polygonal troughs on the uppermost surface. Shadow and MOLA measurements show these layers are ~2 m in thickness. The layers can be exposed in scarps over 30° in slope, but commonly the lower portions of exposed layers are covered by debris with much lower slopes, and also commonly display a patterned surface that can be confused with layering.

2) One or more younger units, approximately 1-2 m thick, that have superposed and filled depressions formed in the older unit, and also formed in local discrete deposits. This unit also has a wide variety of depression types.

Both units show scarp retreat of up to a few m over one Martian year [1].

Erosion and other modification forms: The sprc topography has unique erosional topography [2,3]. Large circular depressions 300 –1000+ m across that cut two to four (perhaps 5) of the layers occur across the sprc. Linear depressions, asymmetric in cross section, usually cutting two-three layers, occur in the central portion of the sprc. Their trends suggest some underlying structural control, while the cross sectional asymmetry may be related to insolation asymmetry. Curled depressions grade into other forms, and show a preferred opening direction toward the north. Other depressions can be irregularly-shaped, and some areas have been largely stripped of the sprc layers by merging depressions. Moat-like depressions occur within some nearly circular forms as well as bounding a variety of mesas and other remnant topography. Moats within depressions show two distinct widths: ~20 m and ~70 m. The latter is indistinguishable from moat widths around mesas and other remnants.

Development of the depressions and deposits: Initiation of many of these forms appears to involve sag and collapse (Fig. 1a,d). Backwasting of the steeper slopes then enlarges the depressions. Changes between 1999 and 2001 indicate some backwasting of the forms of order 1-4 m/ Mars year [1], with a few instances over 5 m. Development sequences of curled depressions can be found, and examples of enlargement almost entirely by collapse are also found (Fig. 1a,d). The sag and collapse features may explain the development of "escher" terrain, whereby an upper surface appears contiguous between different cycles of erosion (Fig. 1d,e).

Most interesting is the development of inverted relief (Fig. 1f-h). The large, scalloped mesas have in some instances collapsed below the level of embaying deposits that in most other instances are lower than the mesa remnants. Different stages of this development can be found in the sprc. The preferred collapse of some materials suggests significant variations in the susceptibility to sublimation of these deposits.

Thin layers preferentially develop pits and other depressions over underlying topography, and on some upper convex slopes. These pits, "peels", and moats indicate modification of overlying deposits by exposure of relief or a critical layer thickness.

Non-uniform deposition is also found in some tongues of material several m in depth and a few hundred m long in restricted areas of the sprc. These appear to be part of the later deposits.

Interpretations: Several different cycles/changes in polar depositional and sublimational regime are indicated:

1). Change from main polar layered deposits to deposition of the sprc: H_20 rich deposits to CO_2 rich ones.

2) Cycles producing layering within the 10 m stack, about 4-5 cycles. Some differences in physical characteristics/ composition.

3) Significant erosion of the deposits in the form of merging depressions and sag and collapse modification.

4) Before or during the subsequent steps, development of polygonal troughs in much of the surface of the thick deposit.

5) Deposition of one or two, ~1- 2 m layers in the erosional topography of the thick deposits, and/or smoothing of surface of a lag deposit left by collapse and backwasting of the layers.

6) Renewed sublimation and collapse of both deposits. Included in this step is the scattered development of inverted relief. This activity may continue at present.

The evident variety of layer types, thicknesses, and cycles of deposition and erosion show there are several combinations of composition and/or texture within these deposits. The sag and collapse suggest a possible role for either absorption of insolation at depth, or a geothermal role in sublimation or other modification of the layers. Loss of substantial porosity might be a part of the collapse sequence. The inverted relief and the other forms surrounding mesa remnants indicate at least one major change in the thermal environment of the layers since major sublimation loss began.

References:

[1] Malin, M. C., M. A. Caplinger, and S. D. Davis (2001). *Science, 294*, 2146-2148. [2] Thomas, P. C. et al. (2000). *Nature 404*, 161-164. [3] Byrne, S., and A. P. Ingersoll (2003). *Science 299*, 1051-1053.

Acknowledgements: Help was provided by Mike Malin, Ken Edgett, Scott Davis, Bruce Cantor, Brian Carcich, Rob Sullivan, Karla Consroe, and Lisa Wei.,.

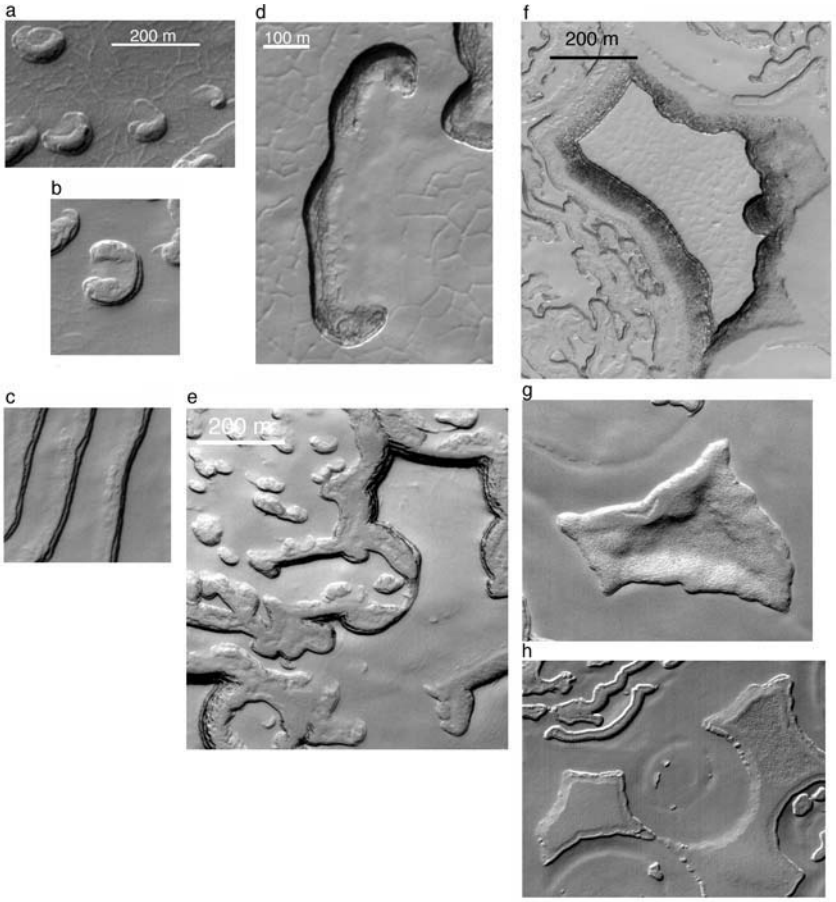

Figure 1a. Sequence of development of curl depressions by collapse and fracture. Illumination is from lower right. b. Curl depression showing ramp from upper surface. Illumination is from lower right. c. Fingerprint depressions; steep on right side, gentle slope on left. Sun is from lower right. Compare gentle slope on left to ramp in Fig. 1b. d. Depression at margin of sag in upper surface. Compare Fig. 1b. Illumination is from upper left. e. Remnant of several layers, near upper right, which tapers to feather edge at lower right. Possible later deposit embays the scalloped margin of the tapering set of layers. Illumination is from lower right. f. Typical remnant of layers, about 10 m above surroundings. Edges are patterned debris. g. Patterned debris from near complete collapse of material such as that in 1f, with overlying deposit (or, less likely, a different form of collapse material). Illumination is from lower right. h. Inverted relief. The scalloped topography of mesas (such as 1f.) has collapsed to a level lower than occupied by embaying materials (note circular feature in middle is high relative to surroundings, illumination is from lower right).

DUST FLUX INTO THE GRÍMSVÖTN SUBGLACIAL LAKE, VATNAJÖKULL ICE CAP, ICELAND, ESTIMATED FROM ICE CORE DATA. Th. Thorsteinsson[1], T. Jóhannesson[2], G. Larsen[3], O. Sigurdsson[1], K.G. Schmidt[4] and M. Forwick[5]. [1]Hydrological Service, Orkustofnun (National Energy Authority), Grensasvegi 9, IS-108 Reykjavik, Iceland. E-mail: thor@os.is, [2]Icelandic Meteorological Office, Bustadavegi 9, IS-150 Reykjavik, Iceland, [3]Science Institute, University of Iceland, Dunhaga 3, IS-107 Reykjavik, Iceland, [4]Niels Bohr Institute, University of Copenhagen, Juliane Maries Vej 30, DK-2200 Copenhagen O, Denmark, [5]Geology Department, University of Tromsoe, N-9037 Tromsoe, Norway.

Introduction. The center of hot-spot volcanic activity in Iceland is located beneath the NW-part of the Vatnajökull ice cap. Continuous melting of the ice cap from below sustains the Grímsvötn subglacial lake; the source of large jökulhlaups which regularly flood regions south of the ice cap [1]. The lake is covered by an ice shelf with an area of 25 km^2 and thickness varying between 100 and 300 m. The bottom of the subglacial lake is covered with sediments of volcanic origin [2], and dust released into the lake by melting of the ice shelf from below is continually being deposited at the lake bed. The Grímsvötn lake has recently attracted the interest of researchers investigating the possible existence of microbial life in Antarctic subglacial lakes and ice covered oceans in the solar system [3].

Ice core study. A 115 m ice core was drilled on the ice shelf in June 2002, concurrently with a thermal drilling that penetrated the ice shelf for geochemical and biological sampling of the subglacial lake [4]. A new core barrel and chips collecting system designed for use in core drilling below the water table in temperate ice was tested with success, and ice core processing involving density measurements, visual-stratigraphic observations, dust measurements and thin section analysis of crystal size was carried out on site.

Density measurements show that the transformation of snow to glacier ice (ρ = 830 kg/m^3) is completed by 16 m depth in the ice shelf, in less than 10 years. The water table in the ice shelf coincides with this transition. Stratigraphic observations reveal the presence of numerous bubble-free melt layers in the core, up to 60 cm in thickness. A 20 cm thick tephra layer from the December 1998 eruption in Grímsvötn was found at 4 m depth, beneath the 2001-2002 winter snow layer, indicating that the entire accumulation of the years 1999-2001 melted during summer. It is thus clear that hiatuses can exist in the annual-layer sequence present within the ice shelf.

The dust concentration of melted 20 cm samples was measured continuously on the core with a *Monilog L* turbidity meter, manufactured by Metrisa Inc. The instrument calculates dust concentrations in ppmv from the intensity of infrared light scattered off dust particles at a 90° angle. Results show that the background dust concentration is in the range 0.3-2.5 ppmv, but peak concentrations of 3-33 ppmv occur at depth intervals varying between 0.5 and 5 m in the core. In most cases, the dust producing the peaks seems to be concentrated in < 1 cm thick layers, which often are visible to the naked eye. Studies on a 100 m core drilled at 1800 m elevation on the Hofsjökull ice cap in Central Iceland [5] have shown that dust peaks in that core are due to windblown dust which originates in nearby deserts and is deposited on the ice cap in late summer. The situation in Grímsvötn is more complicated, since dust from a local source (Mt. Grímsfjall, 2.5 km from the drilling site) can probably be deposited on the ice shelf at all times of the year. Thus, the interpretation of the 40+ dust peaks found in the Grímsvötn core is not straightforward in terms of annual layering, but tephra layers of known ages and a 50 year time-series of winter accumulation from the ice shelf help constrain age vs. depth estimates. The tephra layer from the 1934 eruption is known to lie at ~120 m depth, indicating that the average thickness of annual layers in the uppermost 120 m is 1.8 m. Due to the complicated dynamics of the ice shelf [6], it is not clear how the thickness of the annual layers varies with depth in the lower part, but it seems reasonable to assume that 100-200 annual layers are present within the 280 m thick ice shelf at the drilling site.

The average dust concentration in the ice core is 3.9 ppmv, excluding very high concentrations in layers adjacent to the 1998 tephra layer at 4 m depth. We thus take 4 ppmv (~ 10 ppm by weight) as the average dust concentration in the entire ice shelf, and it seems realistic to assume a similar dust content in the ice within the entire Grímsvötn catchment area. This value is comparable to the dust concentration in Greenland ice dating from the Last Glacial Maximum [7].

From mass-balance considerations, it has been estimated that $4*10^{11}$ kg of ice melt annually by geothermal heat within the Grímsvötn drainage basin, which has an area of 160 km^2 [8]. This corresponds to an ice layer of thickness 2.8 m, melted annually from the base of the glacier. Given the average dust concentration of 10 ppm by weight, the amount of dust released from the melting ice within the entire Grímsvötn drainage basin is $4*10^{11}$ kg$*10^{-5}$= $4*10^6$ kg dust/year. The lake area is ~25 km^2; i.e. ~15% of the area of the entire drainage basin, and thus $0.15*4*10^6$ kg dust/year = $6*10^5$ kg dust are released into the lake

from the shelf per year on average, according to these estimates. The corresponding areal flux is $6*10^5$ kg/$25*10^6$ m^2/year = 0.024 kg/m^2/year.

SEM images of particles from dust peaks in the Hofsjökull ice core show particles mainly in the size range 1-50 μm, made of basaltic volcanic glass together with basaltic crystalline materials and porous tephra grains. No such images are presently available of the Grímsvötn dust particles, but because of the proximity to the subglacially erupted Mt. Grímsfjall and recent eruption products, the proportion of basaltic glass and tephra particles is likely to be high in the Grímsvötn core.

The thin section studies show that average crystal size increases gradually with depth, from ~3 mm just below the firn-ice boundary to ~3 cm in the lowest part of the core. This trend is interrupted in layers containing high amounts of dust, showing that grain-boundary pinning by dust particles, which is commonly observed in polar ice [9], occurs in temperate ice as well. The data on crystal size changes in the core are currently being analysed in the light of new ideas suggesting that habitats for psychrophilic bacteria are present in interconnected liquid veins along three-grain boundaries in ice [10].

References: [1] Björnsson H. (2002) *Glob. Planet. Change*, 35, 255-271. [2] Gudmundsson M.T. (1989) *Jökull*, 39, 1-19. [3] Gaidos E.J. et al. (1999) *Science*, 284, 1631-1633. [4] Lanoil B. et al. (2002) Abstract 03-GM-A-3497-ASM (Am. Soc. Microbiol.). [5] Sigurdsson O. et al. (2002) *NHP Report*, 47, 17-22. [6] Jóhannesson T. (1984). *M.Sc. thesis*, U. Washington, 79 pp. [7] Ruth U. et al. (2003) *JGR*, 108 (D3), 4098. [8] Björnsson H (1988) *Soc. Sci. Isl.*, 45, 139 pp. [9] Thorsteinsson Th. (1997) *JGR*, 102 (C12), 26,583-26,599. [10] Buford Price P. (1999) *PNAS*, 97 (3), 1247-1251.

SOUTH POLAR CRYPTIC REGION REVISTED: THEMIS OBSERVATIONS. T. N. Titus[1], H. H. Kieffer[1], J. J. Plaut[2], P. R. Christensen[3], A. B. Ivanov[2], and the THEMIS Science Team[3], [1]USGS, 2255 N. Gemini Dr., Flagstaff, AZ 86001; email: ttitus@usgs.gov, [2] JPL, Pasadena, CA, [3] ASU, Tempe, AZ.

Introduction: The early part of the Mars Global Surveyor mission provided good TES coverage of the Mars south polar region. These data allow mapping of the polar cap recession, surface and atmospheric temperatures, and albedo features found within the seasonal cap itself [1,2] over L_s = 180° – 270°. During this period, the seasonal south polar cap retreated continuously and asymmetrically around the geographic pole, similar to the observations of Viking in 1976-1977 [3]. A prominent albedo feature on the seasonal cap is a region that appears almost as dark as bare ground, yet remains cold. (See Figure 1.) We refer to this region, generally located between latitudes 85°S and 75°S and longitudes 150°W and 310°W, as the Cryptic region.

Past Observations: A re-examination of the IRTM data revealed that the Cryptic Region was not unique to the TES era, but also was apparent during the Viking IRTM era. (See Figure 2.) Interestingly, Antoniadi [4] observed dark regions forming on the seasonal cap that loosely correlate to the Cryptic region: Depressio Magna (1909) and Depressio Parva (1929). These *depressios* were located at 270° W, 78°S and 166° W, 76°S, respectively.

Analysis of both the TES and IRTM data indicate that the Cryptic region is unique in its thermophysical properties relative to the rest of the cap. The region occupies the same general area from year to year. It is darker and slightly warmer than the rest of the south polar cap. Even though the Cryptic region is slightly warmer, it must still be CO_2-buffered since it remains "cold" for several days.

Spectral analysis of the TES data longward of the 15-micron atmospheric band shows that the Cryptic Region shows less spectral contrast than the rest of the polar cap. This suggests that the region may be composed of "ice," as opposed to snow or frost [5].

The Vent Hypothesis: Since the initial discovery of the Cryptic Region, several surface features, referred to as spiders, fans, and Dalmatian spots on the basis of their appearance, have been seen. The fans and spiders correlate to the location of the Cryptic Region [6]. Kieffer [7,8] suggested that the spiders, fans, and Dalmatian spots are the result of CO_2 vents, caused by basal heating of CO_2 deposits. This can only be possible if the CO_2 is at least partially transparent to visible solar radiation and opaque to thermal IR, thus creating a solid greenhouse effect. The CO_2 would sublimate from the bottom of the ice slab, thus building up pressure until the gas can be released through a vent. The gas would transport dust from underneath the ice, through the vent, resulting in dust plumes. This hypothesis is consistent with past observations.

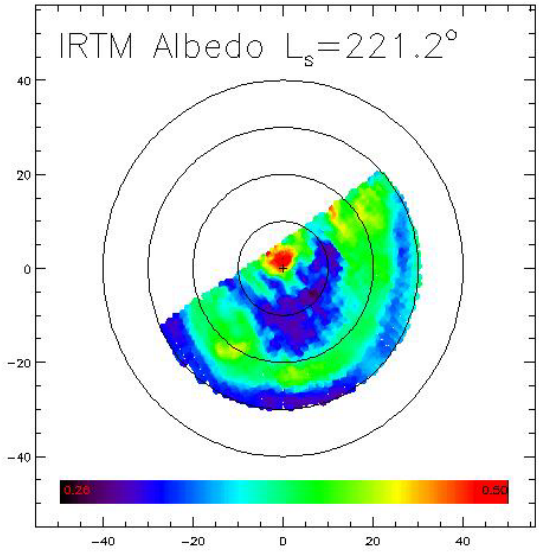

Figure 1: Viking IRTM Albedo Mosaic. This is a mosaic of IRTM visible data taken at L_s = 221.2°. The dark blue feature near the center of the image is the Cryptic region. The latitude lines are drawn at 10° intervals and 0° longitude is up. The region poleward of 65°S is at CO_2 temperatures.

THEMIS Results: THEMIS has the advantage over previous observations in being capable of taking VIS and IR images simultaneously at 18-meter and 100-meter resolution, respectively. Early in the spring, THEMIS observations of Dalmatian spots showed no thermal structure that differentiated the dark albedo areas from the rest of the surrounding seasonal cap. However, by L_s = 206°, thermal structure could be seen. (See Figure 2.) The warmer areas have an increase in brightness temperature of only 5 K over thermally bland areas that are covered by seasonal CO_2 deposits, which is consistent with TES observations at the 3 km scale [9]. These warm areas loosely correlate to the darker albedo areas, as seen in Figures 2 and 3. The spectra of a thermally bland area and an area interior to the three-legged "starfish" show an increase in brightness temperature over the spectral range of 9 μm to 12.5-μm. There are two possible causes for the increase in brightness temperature between these two areas: either the "starfish" surface is warmer than

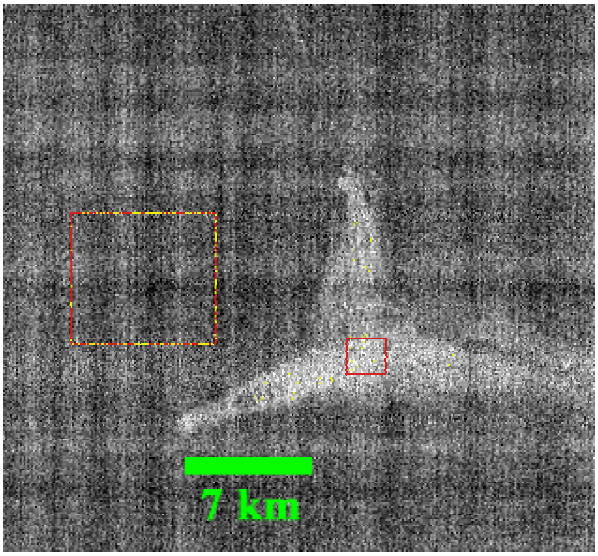

Figure 2: THEMIS IR Image I06707008 (Band 9). This THEMIS IR image shows thermal structure on the seasonal CO2 cap. Spectra were extracted from two locations, the center of the "starfish" and a thermally bland region, representative of seasonal CO_2.

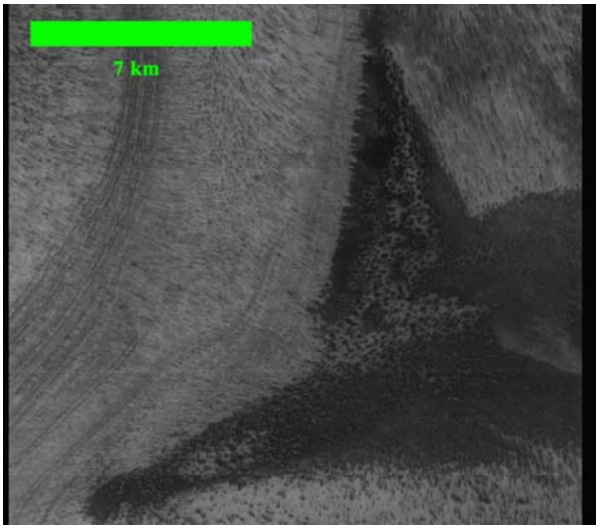

Figure 3: A THEMIS VIS Image V06707009. This THEMIS VIS image shows the same location as the IR image in Figure 2. Notice that the dark albedo region only loosely correlated to the thermal structure seen in Figure 2.

the surrounding area or the local atmospheric opacity is greater than the surrounding atmosphere. If the increase in brightness temperature is due to an increase in the kinetic temperature of the surface, then the spectra have an absorption feature at 11-12 µm. However, if the increase in brightness temperature is due to in increase of atmospheric opacity, perhaps from a nearby dust plume, then the spectra have emission features at 9-10 µm and 12.5 µm. The 9-10 µm spectral region is where atmospheric dust has a peak in opacity. The 12.5-µm region is where water ice clouds have a peak in opacity. The combination of these two spectral peaks in brightness temperature is suggestive of water ice-coated dust grains. Atmospheric emission features are a more plausible explanation of the THEMIS spectra than is an absorption feature at 11-12 µm. The atmospheric opacity explanation of the THEMIS spectra is consistent with the geyser hypothesis.

Summary: We will present the most current THEMIS observations of the Cryptic region. These data, combined with TES data and MOC imaging, will be used to test the Kieffer geyser model.

References: [1] Kieffer, et al. (1998) In LPSC XXIX, Abstract #1481. [2] Titus, T., et al. (1998), BAAS, vol. 30, no. 3, 1049-1050. [3] Kieffer, H.H. (1977) JGR, 82, 4249-4291. [4] Blunck, J (1977) "Mars and its Satellites: A detailed Commentary on the Nomenclature". [5] Hansen,G. (1998) JGR, 104 , 16,471. [6] Piqeux, S. (2003) JGR, Submitted. [7] Kieffer, H. H. (2001) Second International Conf. On Mars Polar Sci. and Exploration, #1057. [8] Kieffer, H. H. (2003), Sixth International Conference on Mars, #3158. [9] Kieffer, H. H. et al. (2000) JGR, 105, 9653.

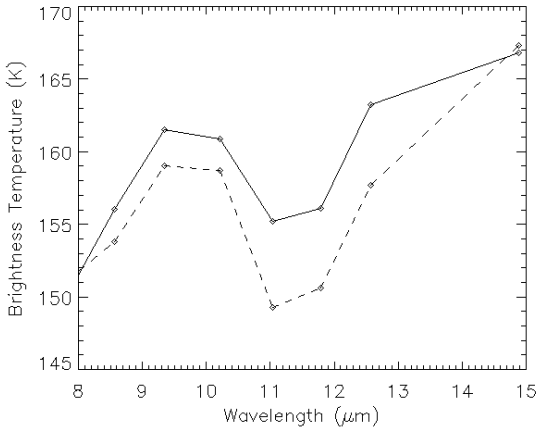

Figure 4: THEMIS IR Spectra. This is a plot of two spectra extracted from THEMIS image I06707008. The solid line is the spectrum extracted from the area inside the small red box (Figure 2). The dashed line is the spectrum extracted from the area in the larger red-yellow box (Figure 2). The 15 µm brightness temperature is an atmospheric temperature.

MODELING THE DEFORMATION OF LOBATE DEBRIS APRONS ON MARS BY CREEP OF ICE-RICH PERMAFROST. E.P. Turtle[1,2], A.V. Pathare[1], D.A. Crown[1], F.C. Chuang[1], W.K. Hartmann[1], J.C. Greenham[3] and N.F. Bueno[2], [1]Planetary Science Inst., 620 N. 6th Ave., Tucson, AZ, 85705, [2]Lunar and Planetary Lab., Univ. of Arizona, Tucson, AZ, 85721-0092 (turtle@lpl.arizona.edu), [3]California Inst. of Technology, Pasadena, CA.

Introduction: A wide variety of mid- to high-latitude surface features on Mars has long been attributed to viscous creep and flow phenomena associated with near-surface ground ice. On the basis of Viking Orbiter images, Squyres [1] identified two classes of creep-related landforms: (1) softened terrain, which results from *in situ* viscous deformation and is particularly evident in impact craters with degraded rims and flattened topographic profiles, and (2) debris aprons, which are produced by mass wasting along escarpments, *e.g.*, lobate debris aprons, lineated valley fill, and concentric crater fill. Such features have been attributed to kilometer-thick layers of permafrost (with upper boundaries less than 200 m deep) at higher latitudes [2], an interpretation that is consistent with recent *Mars Odyssey* GRS observations indicating a high water content very close to the Martian surface [3].

We are using *MGS* MOC and MOLA data to document the structural and topographic characteristics of softened landforms and debris aprons in the Hellas and Noachis regions. By comparing the observed landforms to the results of finite-element models of viscous creep relaxation, which incorporate recent laboratory measurements of ice/rock mixtures [4-6], we can constrain the conditions necessary to allow such deformation on Mars [7,8].

Observations: Debris aprons are broad, gently sloping (~1°-14°) accumulations of material at the bases of escarpments (*e.g.*, Fig. 1). They often exhibit convex-upward topographic profiles (Fig. 1B) and relatively young crater retention ages (1-100 Myr). One concentration of these features is found east of the Hellas impact basin [9]. To look for patterns between the location or nature of mountains and whether or not they exhibit debris aprons, we have characterized debris aprons in a region east of the Hellas impact basin: 30° - 40° S, 240° - 280° W. Using MOLA data we quantified a variety of attributes of mountains in the study region: latitude, longitude, maximum flank slope, total slope, total height, total width perpendicular to the long axis, and basal altitude.

Within this region the only attributes that showed even weak correlations to the existence of debris aprons were latitude and slope, and these were not statistically significant. Debris aprons are more abundant to the south of our study region, which seems consistent with the lower average annual temperatures and annual insolation if near-surface ice (the stability of which is strongly temperature dependent) plays a large role in debris apron formation. Similarly, a correlation between the existence of debris aprons and basal altitude was expected. However, despite a depletion of debris aprons in the portion of the study area within Hellas (westward of ~270°W) no correlation with altitude was observed.

We are in the process of expanding our study area down to 50° south to further investigate the effect of latitude. In this area no debris aprons are found around mountains at low elevation or west of 265° W, *i.e.*, within Hellas. We are evaluating the characteristics of mountains with and without debris aprons outside of Hellas and will combine these observations with those for mountains between 30° and 40° to look for other factors that may control ground ice distribution.

Figure 1: Example of a debris apron around a mountain near Hellas at 45ºS, 255°W. (A) MOC image (M0204416) with the approximate location of the MOLA groundtrack. (B) MOLA topographic profile (orbit 15221), vertical exaggeration ~10.

(A)

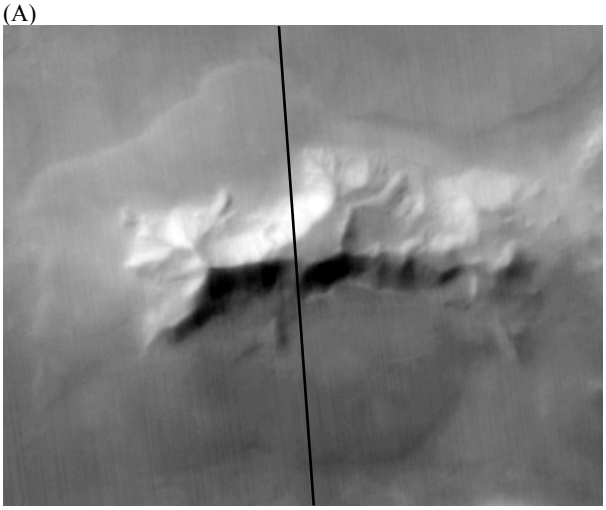

(B)

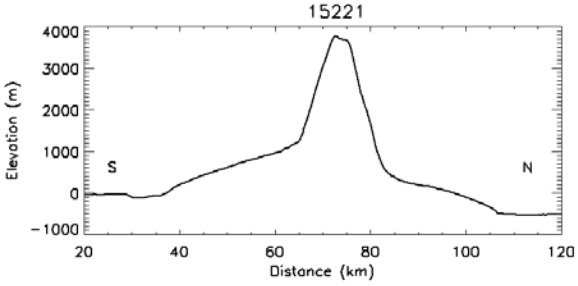

Modeling: We have applied finite-element analysis to investigate the deformation of debris aprons by creep of an ice-rich surface layer. Our models incorporate laboratory measurements of the rheological parameters for dust/water-ice mixtures undergoing dislocation creep and grain size dependent creep [4,5]; both of which are relevant under present Martian conditions: T_{surf} = 200 K [10]; dT/dz = 15 K/km [11,12]. We have built models with initial slopes ranging from 5° - 45° (*e.g.*, Figs. 2-5); slopes as shallow as ~1° have been observed for Martian debris aprons [13,9].

Fig. 2: Cross section of a finite-element model of a 45° scarp with a 1 km thick layer of 30% ice by volume (dark red), before (top) and after (bottom) 1000 yr of dislocation creep.

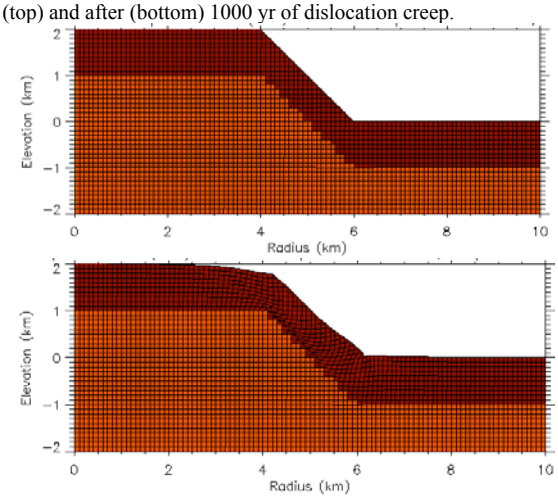

Our simulations demonstrate that the final morphology is very dependent on the initial distribution of the ice-rich material (*cf.* Figs. 3, 4) as well as on the conditions applied at the base of the ice-rich debris. Furthermore, even under present Martian conditions, viscous creep can occur quite rapidly; on timescales of 10^3-10^4 years (Fig. 5). However, if the mobility of the ice is restricted by a surface layer that resists deformation, or the high volume fractions of ice inferred to be present within a ~1 m surface layer [3] does not continue to significant depths, the deformation timescales could be significantly longer. We are also investigating the extent to which blocks of intact rock distributed within the ice-rich regolith [*e.g.*, 14] could serve to increase the deformation timescales.

Fig. 3: Cross-section of a slope of ice-rich material (uniform composition of 30% ice by volume and frictionless basal boundary) after 7500 yr of dislocation creep (basal boundary is frictionless). The solid diagonal line illustrates initial topography which is 34°, near the angle of repose.

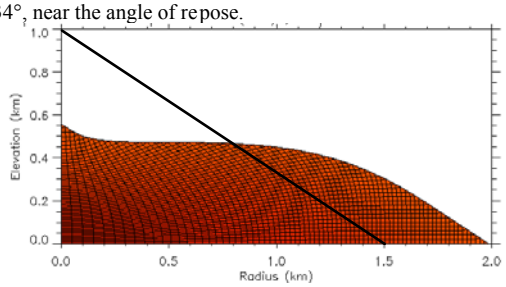

Fig. 4: Cross-section of a 500 m surface layer of ice-rich material (30% ice by volume, dark red) after 7500 yr of dislocation creep (basal boundary is frictionless). The solid diagonal line illustrates initial topography (34°).

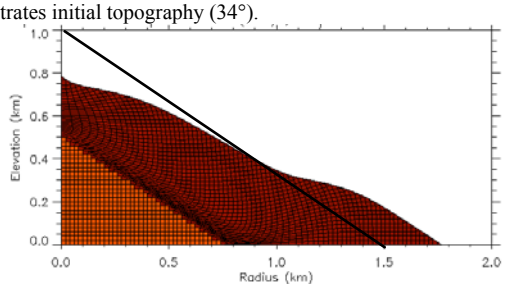

Fig. 5: This (log-log) plot of height-to-length ratio *vs.* time illustrates the rapid evolution of wedge-shaped aprons with initial slopes of 5°, 10°, and 20°. Even slopes as low as ~1° (indicated by the solid horizontal line), which are achieved in significantly less than 10^5 years, continue to deform rapidly.

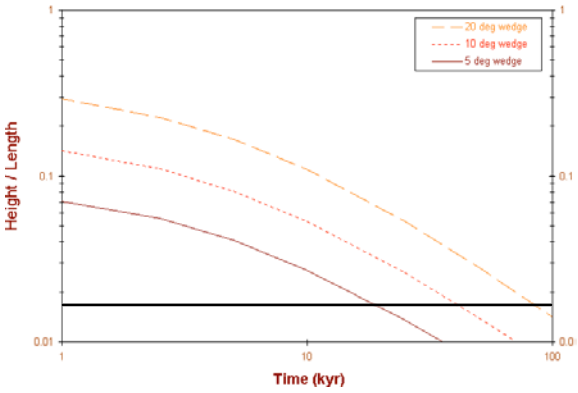

References: [1] Squyres S. (1989) *Icarus* **7**, 139-148. [2] Squyres S. *et al.* (1992) in Mars, Ed. H. Kieffer, Univ. Arizona Press, Tucson, 523-554. [3] Boynton W.V. *et al.* (2002) *Science* **297**, 81-85. [4] Durham W.B. *et al.* (1997) *JGR* **102**, 16293-16302. [5] Durham W.B. *et al.* (2000) Second Intl. Conf. on Mars Polar Sci. and Exploration, LPI Contribution #1057, 28-29. [6] Mangold N. *et al.* (2002) *Planet. Space Sci.* **50**, 385-401. [7] Turtle E.P. *et al.* (2002) *Eos. Trans. AGU, 83*, Spring Meet. Suppl., Abstract #P42A-10. [8] Turtle E.P. *et al.* (2003) *EGS/AGU* EAE03-A-07809. [9] Pierce T.L. and Crown D.A. *Icarus* **163**, 46-65. [10] Martin T.Z. (1981) *Icarus* **45**, 427-445. [11] Schubert G. *et al.* (1992) in Mars, Ed. H. Kieffer, Univ. of Arizona Press, Tucson, 147-183. [12] Clifford S.M. (1993) *JGR* **98**, 10973-11016. [13] Mangold N., Allemand P. (2001) *GRL* **28**, 407-410. [14] Whalley W.B., Azizi F. (2003) *JGR* **108**, 2002JE001864.

SIMULATION OF ATMOSPHERIC CIRCULATIONS OVER THE SUMMERTIME NORTH POLE USING THE OSU MARS MM5. D. Tyler[1] and J. R. Barnes[2], [1]College of Oceanic and Atmospheric Sciences, Oregon State University, dtyler@coas.oregonstate.edu; [2]College of Oceanic and Atmospheric Sciences, Oregon State University barnes@coas.oregonstate.edu.

Introduction: It is important to develop a more thorough knowledge of mesoscale circulations over the residual polar ice caps of Mars. Mesoscale circulations, forced by topography and gradients in the thermal properties of the surface, can significantly modify surface energy fluxes throughout these regions on relatively small scales. Efforts to more completely describe polar weather and climatology, at resolutions greater than those of present day General Circulation Models, must account for the importance of mesoscale circulations. Moreover, a greater understanding of polar mesoscale circulations will assist other investigations into polar processes. This research is the first comprehensive high-resolution attempt to understand the dynamics of the north polar summertime circulation

Mars MM5 Simulations: We have used the OSU Mars MM5 (MMM5) [1] to simulate atmospheric circulations, for northern hemisphere summertime conditions, over the north residual ice cap and southward into midlatitudes. The model was run hydrostatically using a semi-global mother domain, and two-way nesting was used to resolve circulations over Chasma Boreale to a resolution of ~6 km. Three simulations (14 sols each) were performed for L_s values of: 90°, 135° and 160°. Only the final eight sols of each simulation (output centered on L_s values) were used for analysis. Together these simulations allow an examination of how atmospheric circulations change during the entire season that the north residual ice cap is exposed to the atmosphere.

Both the MMM5 and the NASA Ames Mars GCM [2], which is used for boundary and initial conditions, utilize the most current thermal inertia [3], albedo [4] and topography [5] data that is presently available. Our model was tuned to match Radio Science temperature profiles for Ls=135° [6]. The MMM5 was tuned by first setting the visible dust opacity in the model to coincide with TES IR opacities for dust [7], and then by fixing the deepest soil model temperature for ice surfaces (dependent upon albedo) to an appropriate mean climatological temperature (175 K). Subsurface heat flux can play an important role in the residual cap energy budget [8], and this change in the initialization routines of the MMM5 yields simulated residual cap temperatures that match quite favorably with the TES observations without modifying albedo values.

Results: At the time of this writing an analysis of model results is in progress. With three runs, each at multiple resolutions (nesting), we have a 6-D data set. However, there are some results from this analysis that deserve preliminary comment.

Zonal means. Zonal Mean fields from the MMM5 are quite similar with those from the NASA Ames Mars GCM in the lower to middle atmosphere, especially over polar regions when comparing with the coarse resolution results of the MMM5 mother domain (~162 km). At a resolution nine times that of the mother domain (~18 km, two nests in), the winds over the residual cap become well resolved, with zonal mean values at L_s=90° that exceed 10 ms^{-1} near the surface over much of the cap, see Fig. 1. Such wind speeds have been suggested as possibly being required to move the amount of water off the residual cap that was measured by MAWD [9]. By late summer, Ls=135°, mean wind speeds drop to ~5 ms^{-1}, significantly reducing the wind stress on the residual cap.

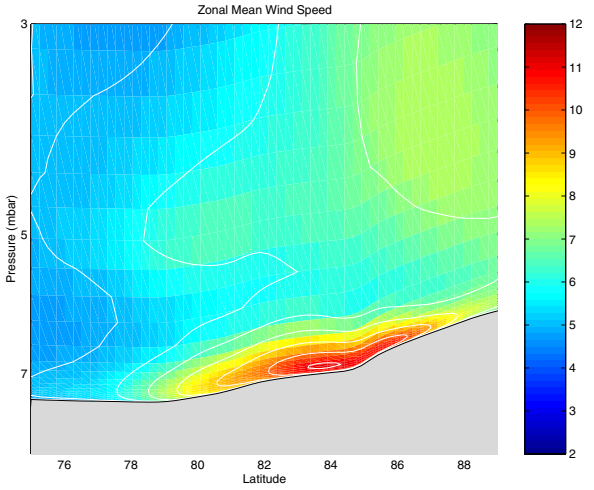

Figure 1: Eight-sol zonal mean wind speeds, for L_s=90°, over the north residual ice cap. The plot was constructed by averaging data on sigma surfaces and then converting the vertical coordinate of the average to pressure. The resolution of this nest is ~18 km.

The zonal mean meridional wind field over the residual cap is weak, as is the zonal mean zonal wind field. At the surface we do observe a weak and fairly shallow off-cap flow, with speeds of ~3 ms^{-1}. Zonal winds contribute most significantly to the zonal mean

wind speeds near the residual cap surface. Aloft, above the residual cap, the zonal mean meridional and zonal winds are negligible, suggesting there is little meridional mixing of the polar atmosphere into lower latitudes. This is only correct in terms of the zonal mean wind fields. For diurnal mean slices at specific longitudes, or for instantaneous meridional winds throughout the course of the day, the results differ dramatically from the zonal means.

Diurnal means and diurnal cycles. Diurnal mean meridional slices of meteorological fields (T, U and V) exhibit a substantial amount of asymmetry from their respective zonal means. As would be expected, we find that some of the strongest off-cap meridional flows are concurrent with Chasma Boreale.

Asymmetries from the zonal mean winds can become surprisingly large at latitudes just south of the residual cap. Certain longitudes exhibit fairly deep northerly or southerly diurnal mean flow (~5 ms^{-1}). At higher altitudes in the modeled atmosphere, asymmetries from the zonal mean meridional flow are also quite pervasive.

Presently we are investigating dynamical mechanisms to better understand the causes for these asymmetric features of the polar circulation in our model. Larger scale dynamics are presumably involved, possibly related to the proximity of Alba Patera and the Tharsis massif. This seems the single most impressive topographical feature that is close enough to be dynamically significant in the polar circulation. A working hypothesis is that stationary features of a larger scale circulation are influencing the smaller scales.

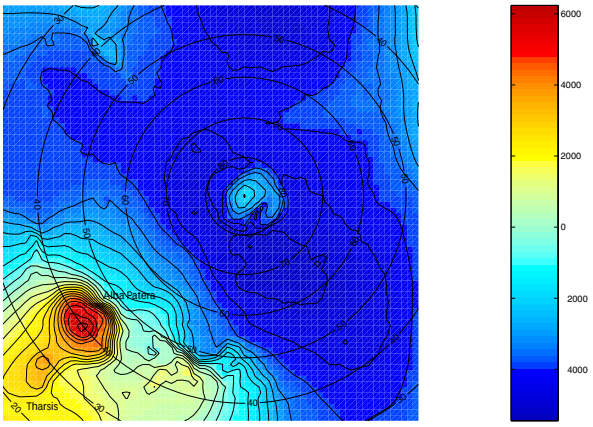

Figure 2: Topography of the ~54 km nest that was used in these simulations (76x76).

An interesting aspect of the polar circulation that we hope to understand is what we have described as "tidal sloshing" [10]. Meridional winds, in the bulk of the atmosphere above the residual cap, reverse direction over the course of the diurnal cycle with a dominant diurnal period. The strength of this effect has longitudinal preference, but it is a pervasive phenomenon over the entire north polar cap in these simulations. The image in Fig. 2 shows topography of the first nest below the mother domain (~54 km); the image is suggestive of why we are suspicious of large-scale dynamical influences related to the proximity of Alba Patera and Tharsis.

Future Direction: This work, when finalized, will complete my Ph.D. studies. Our next effort in this research will be to activate water transport in the MMM5, correctly configure the associated water routines in the model, and revisit these same simulations with the objective of developing a better understanding of the atmospheric pathways through which water is transported southwards off the north residual cap in northern hemisphere summer. There is much to be learned about the present day stability of the residual ice caps using such models, and we look forward to working closely with others interested in investigating the stability and evolution of polar ice deposits.

References: [1] Tyler D. and Barnes J. R. (2002) *JGR, 107,* 10.1029/2001JE001618. [2] Haberle R. M. et al. (1999), *JGR*, *104*, 8957-8974. [3] Mellon M. T. et al. (2002) *LPS XXXIII, Abstract #1416*. [4] Christensen P. R. et al. (2001) *JGR*, *106*, 23,823-23,871. [5] Smith D. E. et al. (1999) *Science*, *284*, 1495-1503. [6] Hinson D. P. et al. (2001) *JGR*, *106*, 1463-1480. [7] M. Smith, *Submitted to Icarus*, (2003). [8] Paige D. A. and Ingersoll A. P. (1985) *Science*, *228*, 1160-1168. [9] Haberle R. M. and Jakosky (1999), *JGR*, *102*, 9069-9083. [10] Tyler D. and Barnes J. R. (2003), *Granada Mars Workshop*.

CHASMA AUSTRALE, MARS: FORMATION BY SUCCESSIVE HEADWARD THERMO–EROSIONAL COLLAPSES.

S. van Gasselt, R. Jaumann, *German Aerospace Center, Institute of Planetary Research (Stephan.vanGasselt@dlr.de).*

Abstract: The development of the south polar Chasma Australe re-entrant has been discussed for several years and a variety of theories including eolian, aquatic, subglacial and tectonic mechanisms have been proposed for its formation. Morphological observations and studies of recent imagery support the idea of successive headward erosion and removal of volatile–rich sub–surface material combined with collapse and eolian blow–out processes.

Introduction: The south polar Chasma Australe is a prominent arcuate elongated trough. Discussed models are formation by eolian processes [2, 3], aqeuous carving [4, 5], subglacial volcanic processes [5, 6] as well as tectonically triggered catastrophic outflow events [1] and basal melting [13]. In this work we provide some aspects to contribute to the understanding of its development. We have mapped the circum–Chasma Australe region on the basis of available imagery (Viking, Global Surveyor MOC, Odyssey THEMIS) at all resolutions and performed morphometric measurements on the basis of Laser Altimetry topographic data (MOLA) to evaluate outflow models proposed for the Chasma Australe development. A detailed description of the general morphology of the Chasma Australe has been provided by [1].

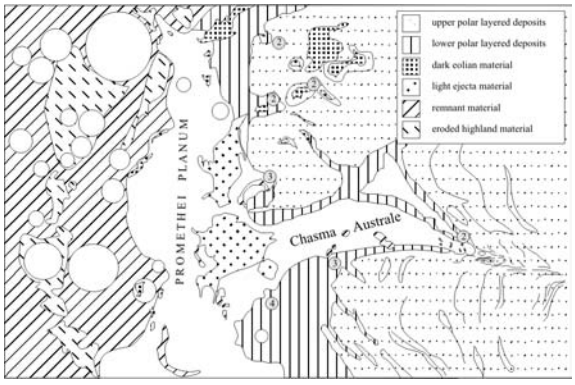

Fig. 1: Map of geomorphologic units of the Chasma Australe region, Promethei Planum and adjacent units. The Chasma Australe system is accompanied by several unlabeled Chasmata (2-4) to the east and west. Several elliptical and circular shaped depressions are located near the heads of secondary (2) re–entrants which indicate identical formation processes. Earlier stages of development (3-4) are presented by small third generation re–entrants. Light material near the terminus of Chasma Australe is connected to impact ejecta, which might be rich in volatiles, as lobate ejecta blankets indicate as well. Lineations south of the head of Chasma Australe.

Geomorphologic and geologic setting: The Chasma Australe is an arcuate and elongated steep sided depression with a length of ≈500 km and a width of 16.5 km at its head and 93 km at its terminus. The Chasma head begins near $-82°$S/90°E and reaches down to 71°S/86°E with an opening angle of $\approx 30°$. It terminates in the Promethei Planum, a large circum-polar basin. The head of Chasma Australe is a well–defined, almost circular depression at an elevation of 2500 m with a depth of 950 m. Inside the U–shaped depression a secondary almost circular depression with a depth of ≈100 m and a diameter of ≈5 km appears. The Chasma terminus is situated at an elevation of ≈1060 m and is marked by a lobate–shaped remnant of possible base rock material.

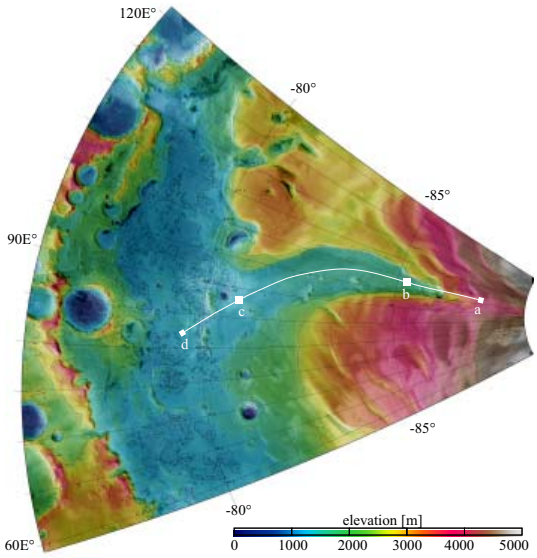

Fig. 2: Topographic map of Chasma Australe, Promethei Planum and adjacent units. Line a-b-c-d marks the profile discussed in the text.

The trough cuts into the Amazonian aged polar layers (Apl), which have been exposed mainly on the eastern flank. The basis of the re–entrant consists of the Hesperian aged Upper and Lower Dorsa Argentae Formations (Hdu and Hdl) [7].

Observations: From its head to its terminus the Chasma covers an area of $\approx 93.6 \cdot 10^3$ km^2. MOLA measurements have shown that $\approx 28.4 \cdot 10^3$ km^3 of material have been removed from the trough. The main trough (profile b:c) has a length of $\approx$ 300 km and slopes with an average angle of $0.06°$ ($S = 0.00112$) (see fig. 3). For comparions reasons we estimated discharge values Q[1] with the help of eight Chasma cross–sections and obtain values ranging from $3.67 \cdot 10^8 m^3 s^{-1}$ to $4.73 \cdot 10^9 m^3 s^{-1}$, depending on the Manning coefficient n (0.03-0.05 [11]) and the definition of the hydraulic radius R. For velocities v we obtained values ranging from $37 ms^{-1}$ to $68 ms^{-1}$. The values show a larger range of estimated peak discharges but they are of the same order as calculations by [1] and estimations for outflow systems in mid latitudes [9]. We obtained higher velocities and slightly larger discharge values. The Chasma floor has a rough small–scale surface texture.

[1](using $v = \left[(g_m RS) \,/\, \left(g_e n^2 R^{-1/3}\right)\right]^{1/2}$according to [11], with velocity $v[ms^{-1}]$, Mars/Earth gravity $g_{m/e}[ms^{-2}]$, hydraulic radius $R[m]$, bed slope $S[-]$, Manning coefficient $n[-]$).

Except for several crater chains in East–West direction only elongated ridges almost perpendicular to the proposed outflow can be observed. We find no streamlined islands as classic features for mid–latitude outflow channels and we have no evidence for outflow–parallel ridges and terraces as a high energetic flow would have caused.

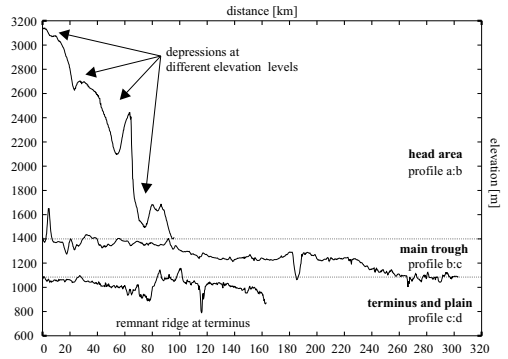

Fig. 3: Length profile of the Chasma Australe head, the main trough and the southern parts of the Promethei Planum.

In an abundance of MOC–NA imagery we observe a pattern of linear, radial and polygonal crack patterns [10] accompanied by cicular and elongated depressions in the vicinity of the Chasma walls and other re–entrants of the south polar region. The crack pattern is aligned parallel to the polar layer outcrops and becomes more densely spaced towards the Chasma walls. These fractures occur mainly near to the southern and eastern (steeper) walls. Linear fracture are connected to elongated depressions and radial fractures are connected with circular depressions. In lower resolution imagery (MDIM resolution) we observe a set of lineaments and large circular depressions south of the Chasma Australe head. The lineaments are exposed polar layer deposits and circum polar troughs which seem to bend in the headward direction of the Chasmata. Fig. 3, profile a:b shows several depressions south of the Chasma head. Each base is situated on a higher elevation level which indicates a headward progressing process of material removal. Near the western walls of Chasma Australe several remnants break through a mantling deposit (s. fig. 2). Between remnant rock and Chasma wall the polar layered deposits remain completely intact.

Conclusions: For the Chasma Australe we propose a successive headward thermo–erosional formation which has been initiated at the Promethei Planum boundary. Sapping processes due to subsurface removal of volatiles could be responsible for collapses and depressions which are aligned in the main directions of several observed Chasmata. Material has been removed afterwards in the direction of the Promethei Planum during several stages similar to the model of supra–glacial erosion by [8]. (1) Although discharge quantities are similar to mid–latitude outflow channels, the general morphology (smoothness, curvature, profile) differs immensly from the well defined known outflow channels. (2) Polar layers remain intact near crucial locations, we have no signs for streamlined islands, groove casts, secondary inner–valley channels or deposits at the terminus towards the Promethei Planum. We find some hints for (3) volcanic influence (crater chains on the Chasma basis and volcanic remnants [12]). Cracks, fissures and small basins near the walls indicate subsurface instabilities in the proximity of the Chasma. The fracture pattern favours the idea of contraction cracking of the surface material, either due to dessication or due to freezing processes of the surface as analogue to terrestrial ice wedge polygonal nets. The depressions indicate either removal of surface material due to deflation, similar to terrestrial pans, sublimation processes or subsurface removal of volatiles and subsequent collapse.

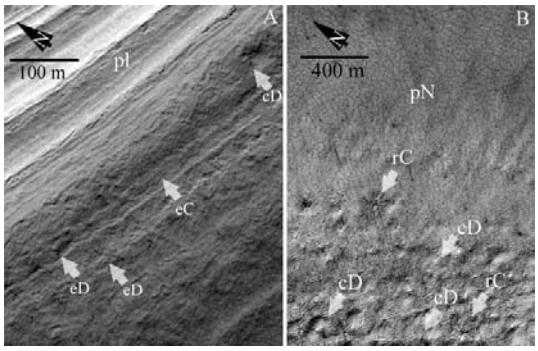

Fig. 4: Selected MOC–NA images at the head of Chasma Australe. (A) E12/02439: The eastern wall shows the layered units (Apl) and presents a pattern of elongated (eD) and circular depressions (cD), as well as elongated cracks (eC) parallel to the layering. (B) E11/01508: Image south of the Chasma's circular head. The polygonal network (pN) is gradually changing to aligned circular depressions and some occurences of radial cracks (rC).

Volcanic processes could be main trigger mechanisms for volatile removal in the subsurface, contraction–cracking and collapse might be bound to this process. Furthermore, eolian transport has a major influence on erosion and mantling the topography. Small–scale cracking and collapse structures are not mantled by eolian material although the overall surface appears very deflated, so even processes of contraction cracking and collapse could occur at present time. Open questions are adressed to the nature of cracking origin (dessication or (CO_2)ice wedges) and the removed material below collapse structures.

References: **[1]** Anguita, F. et al. (2000) *Icarus* **144**, 302-312. **[2]** Cutts, J. A. (1973) *J. Geophys. Res.* **78**, 4211-4221. **[3]** Howard, A. D. (1980) *Icarus* **50**, 161-215. **[4]** Wallace, D. and C. Sagan (1979) *Icarus* **39**, 385-400. **[5]** Clifford, S. M. (1987), *J. Geophys. Res.* **92**, 9135-9152. **[6]** Benito, G. et al. (1997) *Icarus* **129**, 528-538. **[7]** Tanaka K. L. and D. H. Scott (1987) *US Geolog. Surv.*, Map 1-1802-C, Washington D. C. **[8]** Costard, F. et al. (2003) *Lun. Planet. Sci. Conf. XXXIV, #1354*, Houston. **[9]** Komatsu and Baker (1997) *J. Geophys. Res.* **102**, 4151-4160. **[10]** van Gasselt, S. et al. (2003) *3rd Mars Polar Sci. Conf., this volume*. **[11]** Komar, P. D. (1979) *Icarus* **37**, 156-181. **[12]** Ghatan, G. J. and J. W. Head (2002) *J. Geophys. Res.***107**, 10.1029/2001JE001519. **[13]** Fishbaugh, K. et al. (2000) *Lun. Planet. Sci. Conf. XXXI, #1206*, Houston.

DISTRIBUTION AND MORPHOLOGY OF POLYGONS, SOUTH POLAR REGION, MARS. S. van Gasselt, D. Reiß, R. Jaumann, *German Aerospace Center DLR, Institute of Planetary Research, D-12489 Berlin, Germany (Stephan.vanGasselt@dlr.de).*

Abstract: In this work we present a mapping of polygonal patterns at the south pole of Mars between 80°-90°S on the basis of all MOC narrow angle images (up to the current release of E18). We found 750 (out of 6000) MOC narrow angle images showing a variety of polygonal patterns resmebling terrestrial ice wedge polygons. They occur predominately inside circular depressions of the polar layered deposits, circum polar troughs and re–entrants or below slopes.

Introduction: Small–scale polygonal patterns have been observed in Viking Lander imagery [1]. Their morphology and development have often been ascribed to contraction cracking processes, analogous to terrestrial ice wedge polygons and are an indicator for the presence of subsurface water [e.g., 2]. With high resolution imagery from the Mars Orbiter Camera the features have been mapped and classified on a global scale by [3] and [4]. The main focus on analyzing the origin of polygonal patterns has been put on their distribution at southern and northern latitudes of $> \pm 40°$N. In this work we provide a detailed mapping of polygonal patterns at the south pole of Mars (s. fig. 2). The patterns are described on the basis of morphology and distribution.

We have mapped polygonal crack patterns on MOC narrow–angle imagery (up to E -18 release) and combined the results with color–coded MOLA digital elevation models superimposed on the MSSS MOC wide–angle MC–30 imagemosaics.

Geologic Setting and Observations: According to the geologic mapping of [5] the south polar region between 80°S and 90°S consists of the residual ice cap (Api) shifted towards longitudes between 0°W and 90°W. The remaining area is mainly covered by the Amazonian aged polar layered deposits (Apl) with small patches of non–polar related plains unit (s. fig. 1). At longitudes between 265°W and 90°W parts of the upper and lower Hesperian aged Dorsa Argentae Formation are exposed (Hdu, Hdl). The lateral distribution of this unit is equivalent to the area of low elevation (1200 m, blue color, s. fig. 2). At 10°W and between 70°W to 95°W remnants of the undivided Hesperian and Noachian material (HNu) which has undergone degradation processes by removal of ground ice, mass wasting and eolian removal occur.

We observe several regions (marked A–E, s. fig. 1) with clusters of polygonal patterns in MOC imagery. The distinct circum polar distribution (D) of polygonal patterns at 87°S is due to the dense coverage of imagery. The circum polar distribution at 87°S does not continue on the surface of the residual polar cap but spreads along circum polar troughs (C). Especially at longitudes >270°W the polygons are bound to the polar troughs, where (a) the trough material is older than the polar layers at the surface, (b) degradation and removal

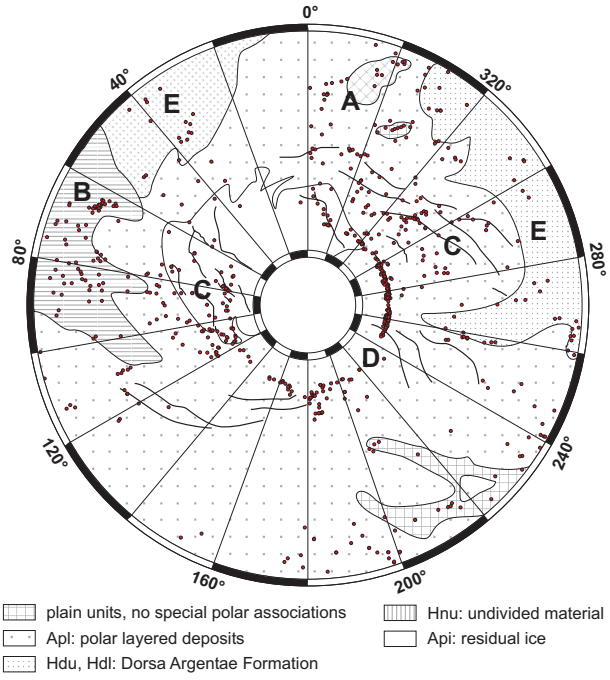

Figure 1: Simplified geologic map of the south polar region between 80°S and 90°S (after [5]) with polygonal crack patterns outside the polar cap. Letters represent areas discussed in the text.

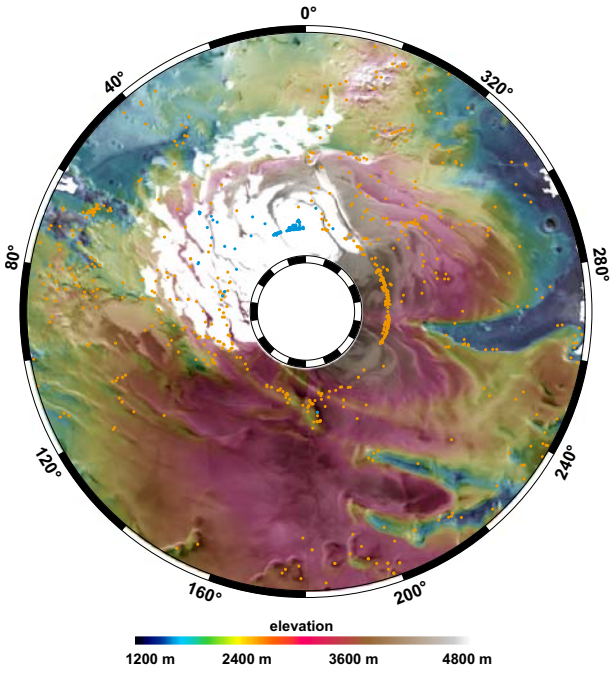

Figure 2: South polar topography and distribution of polygonal crack patterns at the south pole between 80°S and 90°S. Blue dots represent polygonal patterns associated with circular depressions [6] on the residual polar cap.

of material has not yet advanced as far as at the surface, and (c) only a few layers of the polar layered deposits show the typical polygonal pattern. The layers containing polygons are exposed at the Chasma Australe walls, the eastern chasmata, and inside depressions of the polar layered deposits at 180°W to 200°W. At 80°W the circum polar distribution furcates to the north and presents a large cluster of polygonal patterned ground in undivided Hesperian aged units (B).

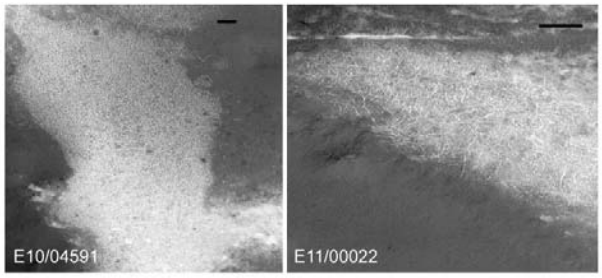

Figure 3: Plains units polygons at 80°S (A on fig. 2). The black bar represents 200 m, north is up. Polygons of the south polar plains units occur predominately in sheltered places at slopes and inside of depressions.

Small quantitites of polygonal terrain is visible on material of the Dorsa Argentae Formation (E), where it is bound to small depressions and rough terrain. Minor clusters of polygonal terrain is exposed adjacent to undivided plain units (A). Polygons related to plains units (A) are randomly orthogonal and highly complex shaped (s. fig. 3). They are degraded and occur south of sheltered slopes or inside depressions. Their diameter varies between 10 to 50 m but reaches up to 80 m. The polygonal troughs are filled with bright material, which might be associated with CO_2 frost [7]. Towards the pole polygons are orthogonal and their shape becomes more distinct with a preferred N–S direction. The polygonal troughs are filled with dark eolian material. Their diameter increase up to 100 to 200 m. Polar troughs related polygons (s. fig. 5) occur on the slopes and inside the troughs.

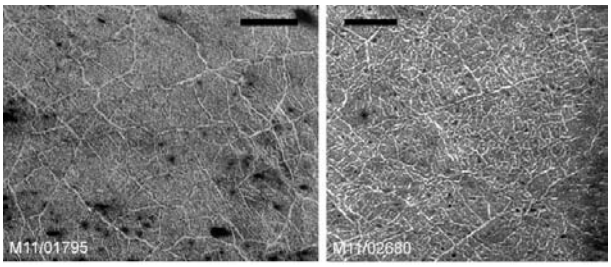

Figure 4: Randomly orthogonal and complex polygons of the Dorsa Argentae Formation (Hdl, Hdu) near 84°W and 80°S. The black bar represents 200 m, north is up.

They have an orthogonal shape and diameters between 10 m to 20 m. Outside the troughs the polygons dissappear below eolian material. Polygons of undivided material near 84°W and 80°S are, similar to the plains units, more complex shaped and randomly orthogonal (s. fig. 4). Polygons exposed at the eroded wall material of the polar layered terrain occur on a few layers only. These polygons are partly degraded but show a distinct orthogonal pattern and sizes in a range of 20-40 m.

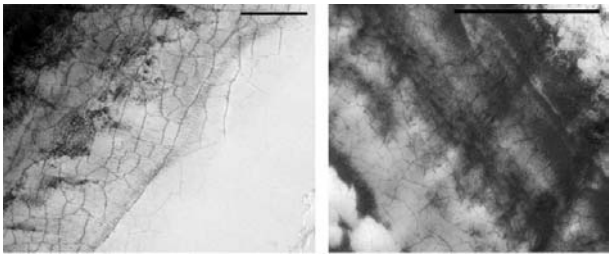

Figure 5: High resolution imagery of polar trough related polygonal networks near 85°W and 86°S. The black bar represents 200 m, north is up.

Conclusions: The distribution of south polar polygons is bound to circum polar troughs, polar re–entrants and depressions where polar layers are exposed (Apl). Polygonal patterns associated with circular depressions can be observed on the polar residual cap. Furthermore, clusters of polygonal patterns are distributed at undivided (HNu) and unclassified plains material. Polygons have a distinct shape and morphology according to their geologic and geomorphologic setting, although transitional morphologies occur in all units. As the distribution is not random at all, surfaces (especially few marker horizons of the layered terrain) showing polygonal patterns might have ages which are valuable to for implications on the past climate. Further research regarding ages is under way.

As far as insights have been provided by MOC, there are major dependencies on parameters like topography, homogeneity of (sub-)surface material, temperature changes, and exogenic degradation processes. Changes in these parameters will affect the growth, size, pattern and distribution of the polygonal networks [8]. Providing a complete coverage, color, and stereo information at high resolution, Mars Express will help to close the remaining gaps and to determine surface and morphologic properties to rule out some of the unknown parameters.

References: [1] T. A. Mutch et al. (1977), *J. Geophys. Res.*, **82**, 4452-4467. [2] M. T. Mellon (1997), *J. Geophys. Res.*, **102**, 25617-25628. [3] R. O. Kuzmin and E. V. Zabalueva (2003), *Lun. Planet. Sci. Conf.*, Houston, #1912. [4] N. M. Seibert and J. S. Kargel (2001), *Geophys. Res. Let.*, **28**, 899-902. [5] Tanaka K. L. and D. H. Scott (1987) *US Geolog. Surv.*, Map 1-1802-C, Washington D. C. [6] Thomas et al. (2000), *Nature*, **404**, 161-164. [7] K. J. Kossacki and W. J. Markiewicz (2002), *Icarus*, **160**, 73-85. [8] A. H. Lachenbruch (1962), *GSA papers*, **70**, New York.

THERMOPHYSICAL PROPERTIES OF MARS' NORTH POLAR LAYERED DEPOSITS AND RELATED MATERIALS FROM MARS ODYSSEY THEMIS. A. R. Vasavada[1], M. I. Richardson[2], S. Byrne[2], A. B. Ivanov[3], P. R. Christensen[4] and the THEMIS Team, [1]Department of Earth and Space Sciences, Box 951567, University of California, Los Angeles, CA 90095-1567, ashwin@ess.ucla.edu, [2]Division of Geological and Planetary Sciences, Mail Stop 150-21, Caltech, Pasadena, CA 90025, [3]Jet Propulsion Laboratory, Mail Stop 168-416, Pasadena, CA 91106, [4]Department of Geological Sciences, Arizona State University, Tempe, AZ 84287.

Introduction: The presence of a thick sequence of horizontal layers of ice-rich material at Mars' north pole, dissected by troughs and eroding at its margins, is undoubtedly telling us something about the evolution of Mars' climate [1,2]—we just don't know what yet. The North Polar Layered Deposits (NPLD) most likely formed as astronomically driven climate variations led to the deposition of conformable, areally extensive layers of ice and dust over the polar region. More recently, the balance seems to have fundamentally shifted to net erosion, as evidenced by the many troughs within the NPLD and the steep, arcuate scarps present near its margins, both of which expose layering.

Viking Orbiter imaging of the NPLD revealed that dark, dune-forming material is spatially associated with NPLD scarps [3]. This material may be liberated from an ice matrix by thermal erosion of the NPLD, either as sand particles or sand-sized aggregates of dust [4]. In either case, the NPLD seems to be a source of material similar in particle size and color to that present in the vast, circumpolar sand sea [3].

Recently, the stratigraphy of the NPLD has been subdivided into two distinct units [5-10]. The upper unit appears to consist of horizontal layers of water ice and a small fraction of dust. Layers are exposed within gently sloping, spiral troughs cut into the cap complex. The lower unit consists of thicker, darker layers with an irregular, platy appearance. It crops out near the margin of the NPLD and within Chasma Boreale. When troughs cut deeply enough to encounter the lower unit, the trough forms are replaced by steep, arcuate scarps. Edgett *et al.* attribute the change in morphology to a lower unit that is less resistant to wind erosion [7].

This stratigraphic sequence has been observed at widely separated locations within the NPLD [6]. If the layering is truly horizontal over the pole, such that the lowest portions of the stratigraphic column crop out in the marginal scarps, it suggests that the erosion of the platy unit uniquely contributes the dark, dune-forming material. Indeed, the platy unit may be an ancient sand sea now covered by the ice-rich, finely layered unit [6], although no bedforms have been found upon it [7].

Optical and thermal infrared (IR) measurements have been used to infer and compare the properties of the different polar materials. For example, Thomas and Weitz compared the color of the dark material near NPLD scarps to material within NPLD layers and within the circumpolar sand sea [3]. Herkenhoff and Vasavada used Viking IR measurements to determine the nature of the dune-forming material and its relationship to other dark, dune-forming materials at lower latitudes [4]. However, such investigations have been limited by the relatively low spatial resolution of Viking color imagery and IR data compared to the spatial dimensions of layers, troughs, scarps, and dune fields. We hope to take advantage of the unprecedented spatial resolution of Mars Odyssey Thermal Emission Imaging System (THEMIS) visible and IR imagery in order to make these inferences and comparisons with the highest possible accuracy (e.g., Figure 1).

THEMIS Observations: To address this science goal, we defined a number of Regions of Interest (ROI) for THEMIS to target as part of the Mars Odyssey Participating Scientist program. We gratefully acknowledge the THEMIS science team and operations staff for acquiring ~100 visible and IR image cubes during Mars' northern summer (L_s 110-160) as orbit tracks intersected our ROIs. The visible image cubes in our data set have five wavelength bands, along-track lengths of ~1000 pixels, and a spatial resolution of 19-38 m/pixel. The IR image cubes have ten wavelength bands and a spatial resolution of 100 m/pixel. The along-track footprint of the IR cubes often begins < 80° latitude, crosses the pole, and terminates < 80° latitude.

Visible Data Analysis: We use these THEMIS data in order to understand the morphology and color/thermal properties of the NPLD and related materials over relevant (i.e., m to km) spatial scales. We have assembled color mosaics of our ROIs in order to map the distribution of ices, the different layered units, dark material, and underlying basement. The color information from THEMIS is crucial for distinguishing these different units (Figure 1), which are less distinct on Mars Orbiter Camera images.

We wish to understand the nature of the marginal scarps and their relationship to the dark material. Co-registered Mars Orbiter Laser Altimeter (MOLA) data provides a measure of scarp morphologies and may help identify the process(es) eroding the NPLD (e.g.,

mass wasting, wind, sublimation). The dark material (or perhaps the platy unit in planar configuration) is present at the feet of many scarps, but does not express dune bedforms there. However, dark material has barchan-type formations when present tens of kilometers away from the scarps [3]. MOLA will help identify the relationship between the spatial distribution of dark material, the presence of bedforms, and the influence of topography.

Thermal Data Analysis: Our next, more ambitious goal is to derive the thermophysical properties of the different geologic materials using THEMIS and Mars Global Surveyor Thermal Emission Spectrometer (TES) data. Such analyses are complicated by the need for atmospheric correction (of both radiatively active CO_2 and dust) and accurate, representative surface temperatures. The latter may be compromised by the footprint size (compared to the areal extent of the material of interest), the influence of topography, and the absolute calibration of the measurement. However, the THEMIS data offer the promise of extending our previous analyses [4] to finer spatial scales and effort will be made to overcome these challenges. In order to derive thermal inertias and thermally derived albedos, we will employ a 1-D, radiative-convective thermal model of Mars surface, subsurface and atmosphere. The model will use simultaneous (or seasonally relevant) TES atmospheric dust opacities, and where possible, include the effects of surface slopes on insolation using MOLA topographic data.

Summary: We hope to understand the geologic evolution of the north polar region by studying the optical and thermophysical properties of polar materials. The primary questions include: what processes control the morphology of the troughs and scarps within the NPLD? What is the nature of the upper and lower NPLD units, as inferred from their thermophysical properties? And finally, what is the nature and source of the dark, dune-forming material?

References: [1] Murray, B. C. et al. (1972) *Icarus*, *17*, 328. [2] Cutts, J. A. (1973) *J. Geophys. Res*., *78*, 4231. [3] Thomas, P. C. and Weitz C. (1989) *Icarus*, *81*, 185. [4] Herkenhoff, K. E. and Vasavada A. R. (1999) *J. Geophys. Res*., *104*, 16,487. [5] Malin, M. C. and Edgett, K. S. (2001) *J. Geophys. Res*., *106*, 23,429. [6] Byrne, S. and Murray, B. C. (2002) *J. Geophys. Res*., *107*, 11-1. [7] Edgett, K. S. et al. (2003) *Geomorph*., *52*, 289. [8] Kolb, E. J. and Tanaka, K. L. (2001) *Icarus*, *154*, 22. [9] Tanaka, K. L. et al. (2003) *J. Geophys. Res.*, *108*, 24-1. [10] Fishbaugh, K. and Head, J. W. (2003), *6th Intl. Conf. on Mars*, abstract 3137.

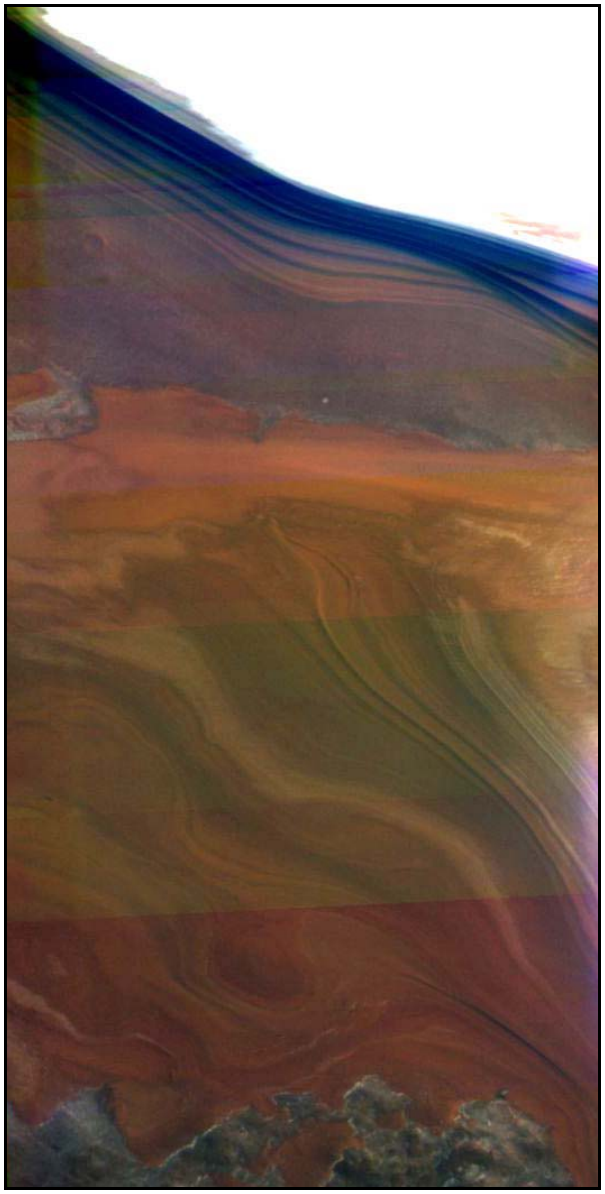

Figure 1. Color composite of THEMIS visible image data showing the north polar residual ice cap (top) and layered materials near the margin of the NPLD. Here the erosion of the deposits appears to "bottom out", exposing the basement terrain underneath the NPLD (best seen along the lower edge of the image). The color information greatly aids this interpretation.

LOW-TEMPERATURE, AQUEOUS ALTERATION OF SOIL IN WRIGHT VALLEY, ANTARCTICA, COMPARED WITH AQUEOUS ALTERATION ON MARS. S. J. Wentworth,[1] E. K. Gibson, Jr.,[2] and D. S. McKay[2], [1]Lockheed Martin Space Operations, C23, 2400 NASA Rd. 1, Houston, TX, 77058 (susan.j.wentworth@jsc.nasa.gov), [2]NASA Johnson Space Center, Houston, TX, 77058.

Introduction: The Dry Valleys of Antarctica are possibly one of the best analogs on Earth of the environment at the surface of Mars. Many types of research have been focused on the Dry Valleys, partly because of the potential application to Mars, and also because of the importance of the Dry Valleys in understanding the characteristics and development of terrestrial polar deserts. In 1983, we published a detailed study [1] of weathering products and soil chemistry in a soil pit at Prospect Mesa, Wright Valley, as a possible analog to Mars. Much more is now known about Mars, so we are re-examining that earlier work and comparing it with newer martian data. The Mars information most pertinent to this work includes (**A**) the strong evidence for recent aqueous activity on Mars reported by [2], along with more recent evidence for present-day, near-surface water ice on Mars [3, 4]; and (**B**) the identification of meteorites from Mars [5] and the subsequent, definitive proof that low-temperature, aqueous weathering has occurred in these meteorites prior to their ejection from Mars [6-8].

Soil column, Wright Valley: The samples used in the Dry Valleys study [1] were taken at irregular intervals from the soil pit shown in Fig. 1. The soil column consists of a permanently frozen zone below ~40 cm depth overlain by an active/seasonally frozen zone.

Results of the Wright Valley work seem to be consistent with what is now known or postulated about Mars. Orbital data indicate the presence of water ice just beneath the martian surface, especially at high latitudes [2, 3].

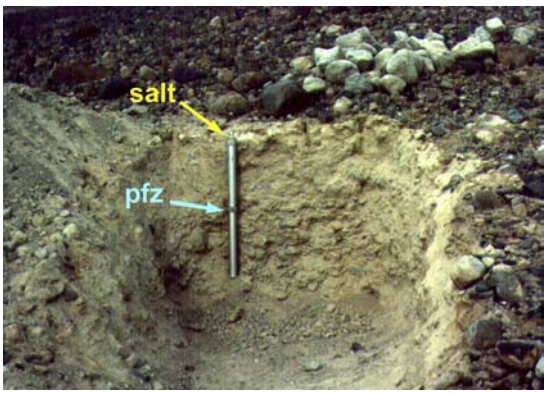

Figure 1: Soil pit, Prospect Mesa, Wright Valley, Antarctica. Drive tube=78 cm long. Yellow arrow points to salt-rich zone just beneath surface (~2-4 cm depth). Top of permanently frozen zone (pfz) is at ~40 cm depth; after [1].

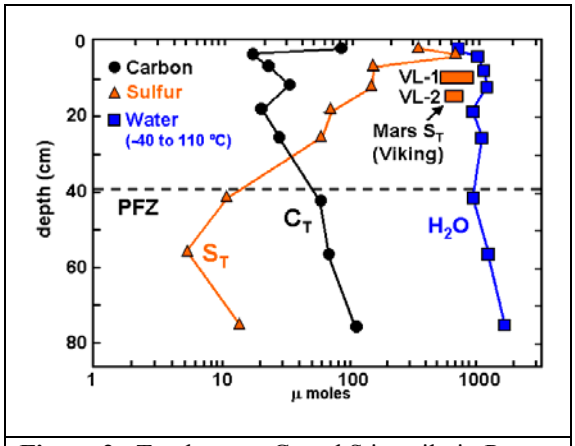

Figure 2: Total water, C, and S in soil pit, Prospect Mesa, Wright Valley; dashed line marks top of permanently frozen zone (pfz); after [1].

Similarly, Fig. 2 demonstrates that the water content (from -40 to +110 deg C) of the Wright Valley soil is much lower at the surface than at depth. This upward decrease in water occurs even within the permanently frozen zone.

In the Wright Valley soil column, water-soluble (salt-forming) species generally increase upward, with a salt-rich zone at ~2-4 cm depth and a dramatic decrease in salts at the surface of the soil (Fig. 3). Mars remote sensing data suggest that total amounts of alteration of original igneous rocks on Mars may be low [3]. The duricrust found just beneath the surface during Viking lander experiments, however, indicate that subsurface salts analogous to those in the Wright Valley soils are likely present on Mars although their possible abundance and distribution are unknown.

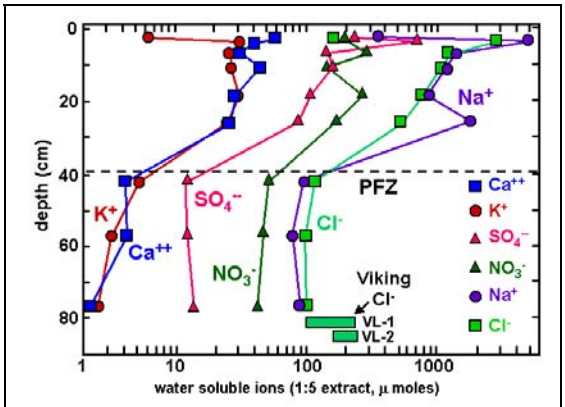

Figure 3: Water-soluble ions in soil pit, Prospect Mesa, Wright Valley; after [1].

Aqueous alteration and secondary phases: SEM studies of the Wright Valley soils [1] showed that aqueous alteration of detrital silicate grains and the formation of secondary phases occurred throughout the soil column, including the permanently frozen zone. Similar features are also present in martian meteorites, and various lines of evidence have shown that some of this alteration occurred on Mars [8, 9]. Examples of typical silicate dissolution in the Dry Valleys soil and a Mars meteorite (Shergotty) are shown in Fig. 4. These features are quite similar to each other. They are typical of chemical weathering of such silicates but are not diagnostic of the mode of alteration. Note that the Wright Valley grain (Fig. 4A) came from the permanently frozen zone of the soil, demonstrating active, although probably slow, alteration processes.

The Wright Valley soil (again, including the permanently frozen zone) and the martian meteorites also contain secondary salts. Secondary carbonates, Ca-sulfate, and halite are found in the Wright Valley soils and the martian meteorites, although not all the meteorites contain all these minerals. A martian origin has been well established for some, but not all, of the secondary phases in martian meteorites. Various means have been used to determine a martian origin for secondary phases; e.g., carbonates in meteorite ALH84001 were quantitatively identified as martian because of their ~3.9 Ga age (ALH84001 itself is 4.5 Ga old) [7]. The origin of many other secondary phases in other meteorites is less certain, however.

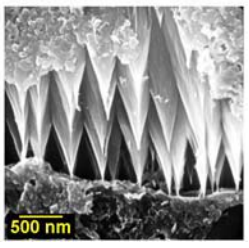

Figure 4A: SEM image of amphibole from Wright Valley soil pit sample WV-221 (permanently frozen zone) showing dissolution features typical for silicates; after [1].

Figure 4B: SEM image of pyroxene from martian meteorite Shergotty (observed fall) with dissolution features and incipient phyllosilicates.

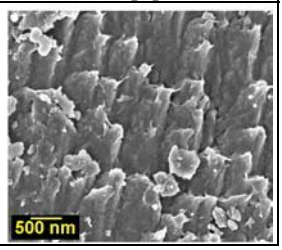

Recent orbital data have suggested the possible presence of a zeolite such as chabazite in Mars dust [10]. Chabazite is present as an authigenic mineral throughout the Wright Valley soil column (Fig. 5) in the Antarctic soil. This is consistent with the suggestion by [11] that chabazite may store water on Mars, especially near the equator. More work is needed to determine whether zeolites are not present in the existing martian samples, or whether they simply have not been found yet.

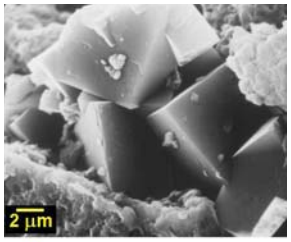

Figure 5: SEM image of authigenic chabazite in Wright Valley soil pit sample WV-221 (permanently frozen zone); after [1].

Conclusions: Aqueous alteration in Mars meteorites and the Wright Valley soil are quite similar with respect to type and degree of weathering of the primary silicates, and also to the nature and distribution of secondary phases. Alteration in the Dry Valleys soils occurs even in the permanently frozen zone, suggesting that similar alteration probably occurs on Mars. Alteration can occur gradually in permanently frozen material because of a liquid-like thin film of water that seems to persist at very low temperatures [12]. Freezing-point depression in brines could also cause weathering at low-temperatures; the salts in the Mars meteorites point to the existence of such brines. The low total amount of alteration of the martian meteorites, along with the presence of secondary phases only in trace amounts, seems consistent with such a process. Transient heating events (e.g., impacts and volcanic activity) have probably been responsible for some weathering on Mars. The Mars meteorites probably do not reflect strong heating events because significant alteration would be expected, at least in close proximity to the heated areas. The seasonal behavior of water ice at the martian poles and possibly elsewhere indicates that water (liquid or vapor) is available for periodic episodes of weathering, even if effects are concentrated mostly on wind-blown dust. Whether or not Mars was once wet and warm, or if it was always cold and dry as suggested by [13], it is clear that weathering and salt deposition have occurred in some form. If the cold, dry Mars model is correct, then the Dry Valleys of Antarctica may be a good analog for most of Mars for most of geologic history.

References: [1] Gibson et al (1983) Proc. LPSC 13, A912-A928; [2] Malin and Edgett (2000); [3] Boynton et al. (2002) Science 297, 81; [4] Christensen (2003) 6th Mars Conf. #3126; [5] Bogard and Johnson (1983) *Science*, 221, 651; [6] Gooding et al. (1988) *GCA* 52, 909; [7] Borg et al. (1999) *Science* 286, 90; [8] Wentworth et al. (2003) *Astrobio*, in revision; [9] Gooding et al. (1991) *Meteoritics* 26, 135; [10] Ruff (2002) *Eos* 83, 1059; [11] Bish et al. (2003) *LPS XXXIV*, 1786; [12] Anderson (1981) *NASA TM 84211*, 292.

LIFE IN PERENNIALLY ICE COVERED LAKES ON MARS - AN ANTARCTIC ANALOGUE

Alex T. Wilson Dept of Geosciences, University of Arizona, Tucson, AZ 86721, USA. (520) 298 5446, email atwilson@U.arizona.edu.

Introduction: As a past member of the New Zealand Antarctic Program, the author spent many summers studying the perennially ice covered lakes in the cold and arid regions of the Antarctic [1 – 5]. This presentation will review what is known about such lakes and conclude that versions of them may exist on Mars. If indeed this proves to be the case, they would be prime sites to look for life. They might also be suitable sites for the construction of a research base, since they would provide a good landing site, water and building material.

Fresh Water Perennially Ice Covered Lakes: It may come as a surprise that large bodies of fresh water can exist in regions where the mean annual temperature is –20 C and below. In the Antarctic, such lakes are possible because some water enters the perennially ice covered lake during a few days each summer. This water flows under an ice cover, which is many meters thick. Water can only be frozen on the bottom of the ice if its latent heat of fusion can be conducted through the overlying ice cover.

The water that enters the perennially ice covered lake flows into the lake and fingers into its appropriate density level. The maximum density for pure water is 4.1 C, which is the temperature of the bottom waters of many of these lakes. For a steady state situation, the amount of water in such lakes (on average) must equal the amount of water sublimed from the ice surface each year, or the lake level will rise or fall until it comes into balance.

During late winter, ice freezes onto the bottom of the perennial ice cover to replace the ice lost during the year. It follows that the thinner the ice, the more ice can freeze onto the bottom of the ice cover. In effect, the ice thickness is a measure of the aridity of the area. Thus the heat input to the perennially ice covered lake comes from the latent heat of fusion of the inflow water and from solar heating.

The very clear ice on perennially ice-covered lakes makes them appear blue. Such an unusual ice cover will give the lakes a low albedo and a "blue ice" color. The ice crystals in the ice cover have been growing for thousands of years. In the case of Lake Vanda [1], perhaps the most studied perennially ice covered lake, the ice crystals are 10 cm across and 3.6 meters long with the c-axis vertical. These crystals act as light pipes and allow the 12 ft ice cover on Lake Vanda to transmit 6% of the total incident solar energy [1]. Because of the unusual crystal orientation of the ice cover, it may be possible to develop methods to confirm the existence of perennially ice covered lakes on Mars.

Can Perennially Ice Covered Lakes Exist On Mars?: The situation on Mars is like the cold arid ice-free areas of Antarctica – only a more extreme version. The temperatures on Martian polar regions are clearly much colder but the relative humidities may be higher. The problem is to find a source of water for Martian perennially ice covered lakes which would replace the sublimation losses from the lake surface. One possibility would be the brine that would be flowing into the sides of the lakes – see discussion below. The origin of the brines entering Antarctic lakes will be discussed and is published [2] [3]. A saturated solution of sodium chloride has a freezing point of –20.7 C and an equilibrium relative humidity of 75%. A better candidate might be calcium chloride: a saturated solution has a freezing point of -50 C (223 absolute) and an equilibrium relative humidity of 45%. Of course in practice, any brine would be a complex mixture. However, it seems feasible to have a situation where in the warmer times of the annual cycle (or at some time in the past) salt brines would flow into a perennially ice covered lake and sink to finger into an appropriate density layer. During the late winter, relatively pure water would freeze onto the bottom of the ice to make up for sublimation from the ice surface. During the summer, the solar radiation would melt voids in the ice, particularly in places where any biological colonies intercept solar radiation. This happens on perennially ice covered Antarctic lakes - see for example references [4] and [5].

Origin Of Brine Needed To Feed The Ice Covered Lakes: The Northern Martian Ice Sheet has probably been in existence for a very long time. The surface of the ice sheet has been losing water by sublimation. This has been made up by the precipitation on the surface by ice crystals. This ice would not be pure water, but would contain small quantities of inorganic salts – e.g. calcium, magnesium and sodium chlorides. Where are these salts today? It is proposed that the more deliquescent of these salts have taken up water and have flowed down-slope into the topographically enclosed drainage basins associated with the ice sheet. Some of these might be expected to contain perennially ice-covered lakes. These lakes may have living things associated with their ice cover, since there would be relatively fresh liquid water at least for part of the annual cycle.

Direct Evidence Of The Existence Of Lakes Associated With The Northern Ice Sheet: Viking Surveyor color satellite photos will be shown (see below) in which a number of ice-blue lakes can be seen occupying the bottom of various enclosed basins. There may even be different kinds of Martian perennially ice covered lakes. For example, one lake appears to be a circular lake analogous to the lakes found on terrestrial icesheets and might be expected to have an ice bottom. Such a lake would be able to acquire water by melting the underlying ice and may contain fresh water. An interesting point is that there appear to be several lakes associated with the Northern Ice Sheet but none are observable in the South Polar Region.

[1]Wilson A.T. and H.W.Wellman Nature **196** 1171-1173.[2]Wilson A.T. Nature **280** 205-208.[3]Wilson A.T. J.Geoph. Rev.,D.V.D.P.,**33** 185-192.[4]Wilson A.T. Ecology **46** 376.[5]Wilson A.T. and H.W.Wellman Nature **196** 1773.

THE NORTHERN ICE SHEET OF MARS WITH FOUR OF THE LAKES ENLARGED

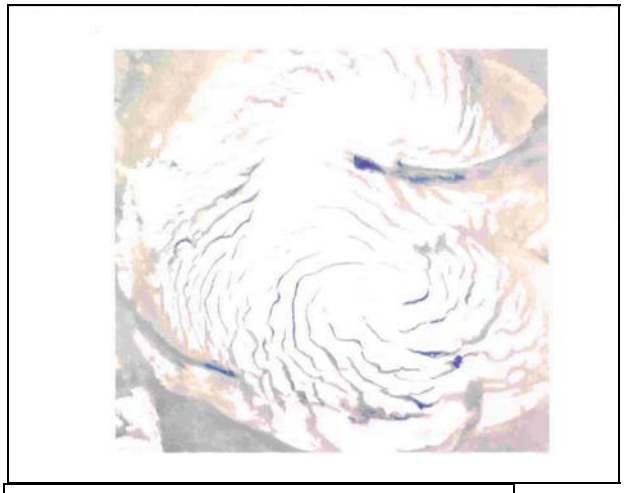

_____100 km_____

_____100 km_____

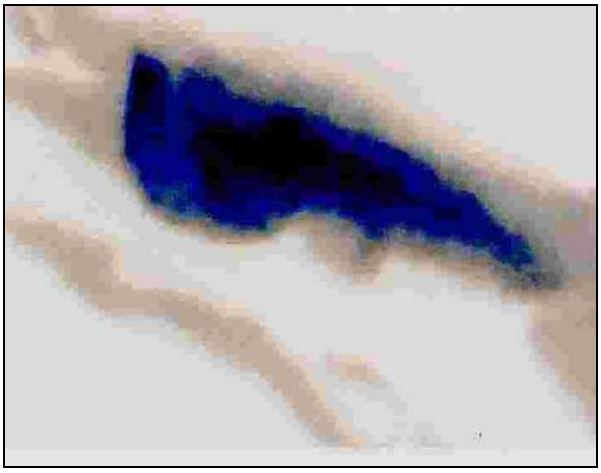

_____100 km_____

THE POLAR REGIONS AND MARTIAN CLIMATE: STUDIES WITH A GLOBAL CLIMATE MODEL. R. J. Wilson[1], M. I. Richardson[2], and M. D. Smith[3], [1]Geophysical Fluid Dynamics Laboratory, Princeton, NJ 08542 (rjw@gfdl.gov), [2]Division of Geological and Planetary Sciences, MC 150-21, California Institute of Technology, Pasadena, CA 91125 (mir@gps.caltech.edu), [3]NASA Goddard Space Flight Center (Michael.D.Smith@gsfc.nasa.gov).

Introduction: Much of the interest in the polar regions centers on the fact that they likely contain the best record of Martian climate change on time scales from years to eons. This expectation is based upon the observed occurrence of weathering product deposits and volatile reservoirs that are coupled to the climate. Interpretation and understanding of these records requires understanding of the mechanisms that involve the exchange of dust, water, and carbon dioxide between the surface and atmosphere, and the atmospheric redistribution of these species. We will summarize our use of the GFDL Mars general circulation model (MGCM), to exploration aspects of the interaction between the global climate and the polar regions. For example, our studies [1] have shown that while the northern polar cap is the dominant seasonal source for water, it can act as a net annual source or sink for water, depending upon the cap temperatures and the bulk humidity of the atmosphere. This behavior regulates the annual and global average humidity of the atmosphere, as the cap acts as a sink if the atmosphere is too wet and a source if it is too dry. We will then focus our presentation on the ability of the MGCM to simulate the observed diurnal variations of surface temperature. We are particularly interested in assessing the influence of dust aerosol and water ice clouds on simulated surface temperature and the comparison with observations. Surface thermal inertia and albedo are critical boundary inputs for MGCM simulations. Thermal inertia is also of intrinsic interest as it may be related to properties of the surface such as particle size and surface character.

Model: The GFDL Mars general circulation model simulates the circulation of the Martian atmosphere from the surface to roughly 90 km [2]. The MGCM includes parameterizations for radiative transfer associated with CO_2 gas and for aerosols. An arbitrary number of aerosol populations can be transported by the simulated circulation. Dust may be injected at the surface using a prescribed rate and spatial distribution. We have recently added a dust source scheme that associates injection with resolved wind stresses and parameterized dust devil activity. This scheme allows the seasonal cycle of air temperatures and dust to match observations well at times when large-scale dust storms are not occurring. The model has also proven capable of simulating global dust storms with interannual variability in size and timing of occurrence. A potential source of memory for interannual variability is the spatial distribution of dust on the surface, as suggested by spacecraft and telescopic observations of interannual albedo variations. An ongoing line of research is considering the coupling of injection and sedimentation to the surface budgets of dust to investigate their role in interannual variability and assess net transport of dust onto the polar caps.

The water cycle is represented by surface ice and regolith water reservoirs, atmospheric transport and ice cloud formation [1,3]. The optical properties of predicted ice clouds can be passed to the radiative heating codes, allowing cloud radiative feedbacks and dust-water ice interactions to be examined.

Surface Temperature:

The daily and seasonal variation in surface temperature is a central element in the description of the martian climate. In the case of an optically thin atmosphere, surface temperature provides the bottom boundary condition that fundamentally influences the profile of overlying atmospheric temperature. The low thermal inertia of the Mars surface allows for the large seasonal variation in diurnal-mean surface temperature that reflects the seasonal migration of the subsolar latitude and the annual variation in insolation due to the eccentric orbit. We have used MGS TES surface temperatures and thermal inertia estimates [4,5] to derive thermal inertia and albedo maps suitable for use in the MGCM. It is important to note that estimates of thermal inertia must account for atmospheric opacity due to dust and water and CO_2 ice clouds. These effects are significant in the polar regions and will influence the characterization of the polar surfaces. By using relatively coarse spatial resolution compared to [4], we can more readily trade off spatial resolution for temporal resolution and relate the evolution of observed morning and afternoon temperatures (and thermal inertia estimates) to variations in atmospheric opacity.

Figure 1 shows the seasonal evolution of zonally-averaged daytime (2pm) surface temperature (contoured) from a reference simulation representing relatively clear sky conditions. There is a large seasonal variation in temperature that reflects the seasonal migration of the subsolar latitude and the annual variation in insolation due to the eccentric orbit. The advance and retreat of the polar CO_2 ice caps approximately follows the 150 K isotherm. It is apparent that very strong temperature gradients develop along the retreating edge of the polar caps as spring advances into summer in each hemisphere. These gradients likely give rise to

strong local thermal wind systems that evidently are associated with observed local dust storm activity along the cap boundaries [*6*].

Figure 1 also shows the difference between zonally-averaged TES surface temperatures and those from a reference MGCM simulation. This figure clearly highlights the seasonal changes of observed temperatures that may largely be attributed to variations in atmospheric opacity. Temperature differences are minimal during the relatively clear NH spring/summer season when the atmospheric opacity assumed in the simulation most closely approximates that of the actual Mars atmosphere. The effects of a regional scale dust storm at L_s=225° in the first mapping year and a major, planet-encircling dust storm at L_s=185° in the second year are evident. A dusty atmosphere leads to an increase in morning temperature and a decrease in afternoon temperature.

There are systematic temperature differences in the vicinity of the polar caps. These are due, in part, to errors in simulating the polar cap latitude. Significant temperature differences are also due to the presence of dust and polar hood clouds in the vicinity of the polar caps. The aphelion season tropical water ice cloud has a clear influence on apparent tropical nighttime temperatures. We will show how simulated temperatures depend on atmospheric opacity. In a related manner, we consider how atmospheric opacity affects the determination of surface thermal inertia.

References: [1] Richardson, M. I. and Wilson, R. J. (2002) *JGR 107(E5)*. [2] Wilson, R. J. and Hamilton, K. (1996) *J. Atmos. Sci., 53,* 1290-1326. [3] Richardson, M. I., Wilson, R. J. and Rodin, A.V. (2002) *JGR 107(E9)*, 5064. [4] Mellon et al., (2000), *Icarus, 148*, 437-455. [5] Christensen et al. (2001) *JGR 106*(E10), 23823-23872. [6] *Cantor et al*. (2001), JGR 106, 23653-23687.

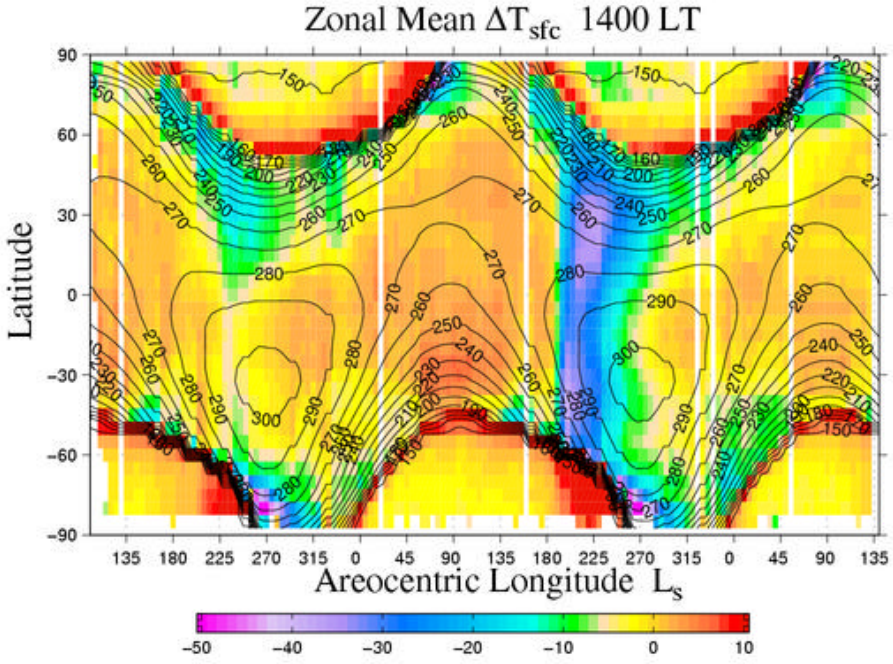

Figure 1. The seasonal evolution of zonally-averaged afternoon surface temperature anomaly derived from TES spectra. Afternoon temperatures nominally correspond to 1400 LT. Predicted surface temperatures from a MGCM simulation employing a low (τ=0.1) atmospheric dust column have been subtracted from the observed surface temperatures to highlight changes in surface temperature due to atmospheric opacity. The simulated surface temperature is contoured. A dusty and/or cloudy atmosphere leads to a decrease in observed afternoon temperature (and an increase in observed morning temperature) relative to the reference simulation. The effects of a regional scale dust storm in the first year (L_s=225°) and a major, planet-encircling dust storm in the second year (L_s=185°) are evident.

ICE KEEL SCOUR MARKS AND ICE FLOE GROUNDING STRUCTURES IN KASEI VALLES AND ECHUS CHASMA. Christopher Woodworth-Lynas and Jacques Yves Guigné, Guigné International Ltd. 685 St. Thomas Line, Paradise, Newfoundland, CANADA A1L 1C1 709 895 3819 chriswl@guigne.com

Introduction: We present further new observations from analyses of Mars Global Surveyor Mars Orbiter Camera images of surficial features interpreted to be the result of interactions between the keels of floating ice masses on submerged sediment [1]. The surface morphology of scour marks typically comprises a curvilinear trough from which seabed material has been ploughed to the sides by the entrenched, moving ice keel, to form two co-linear berms of excavated material.

Background: Scour marks are the seafloor tracks made by floating ice masses as their keels mechanically plough into soft sediments of lake, river or ocean floors. On Earth scour marks are ubiquitous features on the seafloors of the modern Arctic and sub-arctic regions and on the seafloor of the continental margin of Antarctica.

Scour marks commonly survive the transition from submergence to exposure above water level and ancient features are commonly seen, over large areas of southern Manitoba and parts of southern Ontario formerly occupied by glacial Lake Agassiz and glacial Lake Iroquois [2,3]. They are also found on several large islands of the Arctic Archipelago (e.g. King William Island, Victoria island) and are readily identified from aerial photographs. The relic Arctic features were formed in areas formerly submerged below sea level some 10,000 years ago. Scour marks preserved in Pre-Cambrian, Ordovician and Carboniferous/Permian age glacimarine sediments have also been identified on exposed bedding plane surfaces in several localities worldwide [4].

On Earth scour marks form today in water depths from < 5 - 500 m, and fall in the range < 100 m to several kilometers long, 5 - 100 m wide and < 1 - 5 m deep (exceptionally 25 m).

In a preliminary analysis [1] we examined several hundred high-resolution narrow angle images acquired by the Mars Orbiter Camera (MOC). We searched for ice keel scour marks to the margins of Chryse Planitia in the vicinity of an ancient shoreline, Contact 2, proposed by [5] and largely substantiated [6], and to the valley floor regions of the six great valley systems that empty into Chryse: the Mawrth, Ares, Tiu, Simud, Maja and Kasei Valles systems. We chose these regions because floating ice masses, either river ice from the valleys, or sea ice would likely ground and scour in the littoral waters of a river mouth and near-shore region, and that traces of this activity may be preserved on bedding surfaces.

Present work and description of Martian features: We have extended our analysis and interpretation to include much of Echus Chasma (Figure 1) where we have identified features interpreted as multi-keeled scour marks and in one place a zone of multiple, parallel scour marks related to the movement of ice keels locked in a floating ice canopy (Figure 2).

***Networks of Parallel sided Troughs with Berms*:** On the flat valley floor of Kasei Valles and in Echus Chasma we have found networks of curvilinear, intersecting, parallel-sided troughs that meander and intersect with no consistent orientation. The troughs typically are at least 1 km long and some exceed 3 and 4 km and range in width from 10 – 50 m. By observing sun shadows it is possible to distinguish narrow ridges, or berms, on one or both sides of most troughs. In places *multiple, overlapping sub-parallel trough*s coalesce into wide (100 - 300 m), irregular-sided grooved and ridged surfaces.

***Ridge-bounded regions*:** Associated with the troughs are poorly- to moderately well-defined irregular to rounded, smooth, low albedo regions, the margins of which are defined by low continuous ridges. These ridge-defined smooth areas range in size from 200 to 600 m, exceptionally up to 950 m. They may occur as solitary features, but more commonly occur in groups forming jig-saw-like ridge networks. In Echus Chasma these ridge-defined features are larger (in the range 0.5 to 1.0 km) and individual features may contain smaller, well defined jigsaw-like groups of sub-circular regions, that are also defined by ridges of a smaller scale than the larger feature in which they are contained.

In Kasei Valles the *parallel-sided troughs with berms*; the *multiple, overlapping sub-parallel troughs*; and smooth *ridge-bounded regions* are restricted in their occurrence to the lowest and flattest portion of the valley floor (Figure 1) and do not occur at or east of the vicinity of Sharanov crater and are not found on any of the elevated, older grooved surfaces of the Kasei system.

Ridge-defined smooth areas are considerably more common, and of larger scale, in the much wider, flat regions of Echus Chasma. Parallel-sided troughs with berms are less common but multiple troughs (Figure 2) and closely-spaced parallel troughs were found here.

Interpretation: We interpret the small-scale troughs on the floor of the Kasei Valles system as ice keel scour marks made by the bottom-touching keels of floating ice floes. We interpret the associated ridge-defined low albedo regions as grounding pits made by stranded tabular floes. The megaripple-like surfaces on

which the scour marks and grounding pits appear to have formed in the lower Kasei Valles during a period of strong unidirectional down-valley currents. There may have been floating ice present and ice scouring may have occurred during megaripple formation but all traces have been erased by the migrating ripples. As the strong currents associated with the megaripples waned, ice scour marks and ice floe grounding pits formed and were preserved. The meandering tracks of the scour marks point to a significant decrease in unidirectional flow, and suggest that winds may have played a significant role in driving the scouring floes.

We interpret the wide lanes of multiple, overlapping sub-parallel troughs as zones of linear shear in the ice canopy (Stamukhi zones), which are typically regions of intense ice keel scouring of the seafloor e.g. [7, 8].

Discussion and implications: The preserved traces of ice keel scour marks and ice floe grounding pits are restricted to the surface of stratigraphic Kasei unit 2. The scour marks are therefore of early Amazonian age. Scour marks demonstrate:

1. the former presence of a water body;
2. the water body must have been at least seasonally, or perhaps permanently, covered by ice floes;
3. the water area must have been large enough for wind and current to drive the floes forward during ice/seabed interaction.

References:

[1] Woodworth-Lynas, C.M.T. and J.Y. Guigné. 2003. Ice keel scour marks on mars: evidence for floating and grounding ice floes in Kasei Valles. 6th International Conference on Mars. Pasadena, July 20-25th.

[2] Gilbert, R.J., Handford, K.J. and Shaw, J., 1992. Ice scours in the sediments of glacial Lake Iroquois, Prince Edward County, eastern Ontario. Geographie physique et Quaternaire v. 46, 189-194.

[3] Woodworth-Lynas, C.M.T. and J.Y. Guigné. 1990. Iceberg scours in the geological record: examples from glacial Lake Agassiz. In, Glacimarine environments: processes and sediments (J.A. Dowdeswell and J.D. Scourse, eds.). Geol. Soc. Spec. Pub. No. 53: 217-233.

[4] Woodworth-Lynas, C.M.T. and J.A. Dowdeswell. 1994. Soft-sediment striated surfaces and massive diamicton facies produced by floating ice. In: Earth's Glacial Record (Eds. M. Deynoux *et al*.) Cambridge University Press: 241-259.

[5] Parker, T.J. , D.S. Gorsline, R.S. Saunders, D.C. Pieri and D.M. Schneeberger. 1993. Coastal geomorphology of the Martian northern plains. JGR, 98: 11061-11078.

[6] Ivanov, M.A. and J.W. Head. 2001. Chryse Planitia, Mars: Topographic configuration, outflow channel continuity and sequence, and tests for hypothesized ancient bodies of water using Mars Orbital Laser Altimeter (MOLA) data. JGR, 106 (E2): 3275-3295.

[7] Barnes, P.W., D.M. Rearic, and E. Reimnitz. 1984. Ice gouging characteristics and processes, In, The *Alaskan Beaufort Sea - Ecosystems and Environments.* Academic Press, Orlando: 185-213.

[8] Reimnitz, Erk, and P.W. Barnes. 1974. Sea ice as a geologic agent on the Beaufort Sea shelf of Alaska: In, *The Coast and Shelf of the Beaufort Sea,* edited by J.C. Reed, and J.E. Sater, Arctic Institute of North America, Arlington, VA: 301-351.

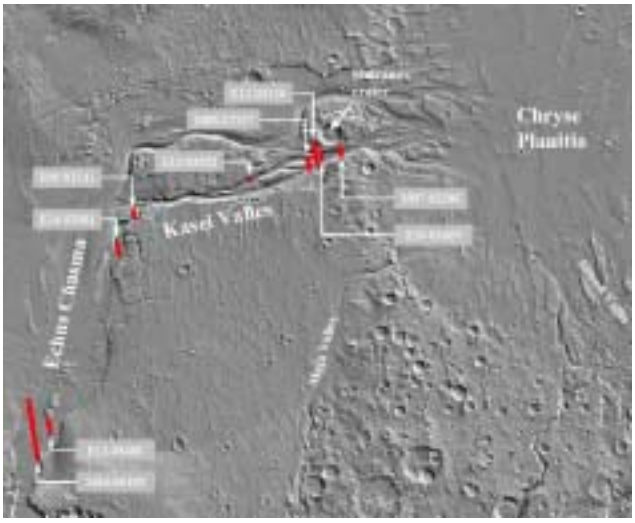

Figure 1 Relief map of Kasei Valles with location of selected MOC images that show ice scour marks and ice floe grounding pits. Context relief image from the Mars 2001 Odyssey THEMIS website (http://themis-data.asu.edu/).

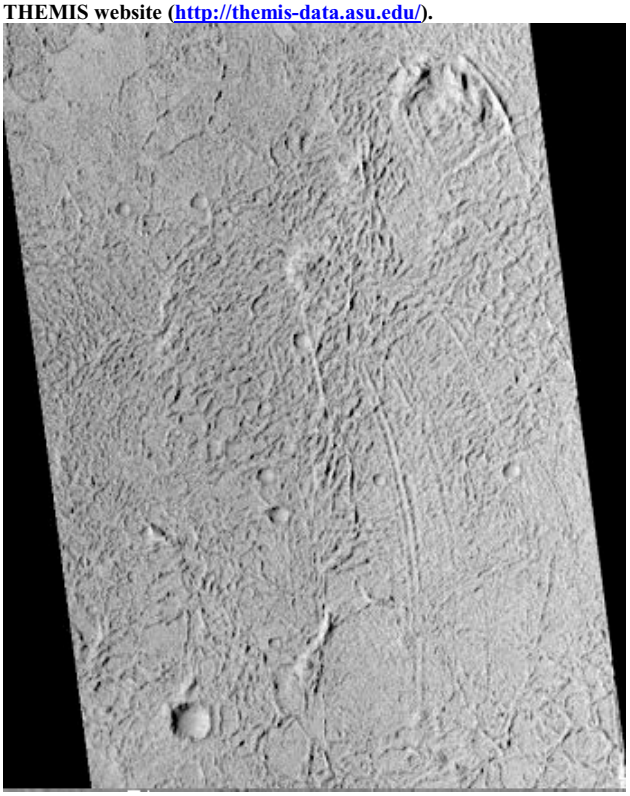

Figure 2 MOC image (southern Echus Chasma) of a 2 km-wide group of curved, wind-driven ice keel scour marks terminating in transverse ice-push ridges. MOC image M14-00193. Scaled pixel width: 11.6 m; Scaled image width: 2.96 km.

ORIGIN OF MGS-TES SURFACE COMPOSITIONS IN THE NORTHERN PLAINS AND POLAR REGION OF MARS. M. B. Wyatt[1] and K. L. Tanaka[2], [1]Department of Geological Sciences, Arizona State University, Tempe, AZ 85287 (michael.wyatt@asu.edu), [2]U.S. Geological Survey, Flagstaff, AZ 86001 (ktanaka@usgs.gov).

Introduction: The largest extent and highest concentrations of the MGS-TES derived Surface Type 2 (ST2) spectral unit, interpreted as an andesitic [1,2] and/or partly altered basaltic composition [3], are mapped in the low-albedo northern lowlands and circumpolar sand seas of Mars [1]. In this study, we examine the relationships between distributions of TES-derived surface compositions and mapped geologic units in the northern polar regions of Mars and integrate Viking, MGS-MOC and -MOLA and MO-THEMIS datasets to constrain theories of the composition, origin, and evolution of these materials.

MGS-TES Background: Studies of low-albedo regions on the martian surface using atmospherically corrected thermal emissivity data from the MGS-TES have identified two distinct global surface spectral signatures [1, 4-6]. The Surface Type 1 (ST1) spectral end-member has been interpreted as an unaltered basalt [1-2, 4], while the ST2 spectral end-member has been variously interpreted as an andesitic [1,2] and/or partly altered basaltic composition [3]. The ST1 surfaces roughly form an equatorial band, restricted to southern highlands and Syrtis Major regions and a few local depostis in the northern plains, capped with ST2 surfaces at mid-latitudes and high-latitudes [7,8]. The transition from ST1 to ST2 compositions at southern high-latitudes appears gradual with no obvious distinguishing boundaries, unlike the topographic dichotomy to the north where plains materials are dominated by ST2 compositions [8]. Detectable abundances of local hematite [e.g. 9], orthopyroxene [e.g. 10], and olivine [e.g. 10] have also been identified in equatorial regions where ST1 basaltic compositions dominate surface units. The mapped distributions of ST1 and ST2 materials indicate that surface compositions are not well correlated with crustal thickeness [8,9].

Northern Plains Geologic Relations: The ST2 surfaces in the northern lowlands correspond with the distribution of low-albedo surfaces, which surround Planum Boreum, cover vast expanses of Vastitas Borealis, and extend in some regions south of 30°N. These surfaces occur on a variety of geologic units, including the VBF, other plains materials, dissected and rugged volcanic flows of Tharsis and Elysium,and circumpolar dunes (Fig. 1).

Part of the ST2 signature in the northern lowlands may be related to chemical weathering caused by water at the surface during periods of high obliquity. The high southern latitudes of Mars (>30°S) also display ST2 materials and do not appear to be generally related to outcrops of volcanic rocks. The correlation with high latitudes may be indicative of modest chemical weathering of basaltic rocks (type ST1) in which liquid water has been present on and near the surface at least periodically, perhaps at times of high obliquity beneath snow packs [11]. The same explanation may hold true for basaltic rocks in the northern plains. However, the TES signature in the northern plains indicates a higher ST2 abundance than the south polar region. Given also the relative youth of northern plains surfaces vs. the southern highlands, it would appear that this obliquity-related mechanism cannot fully explain the northern plains ST2 signature.

In the plains surrounding Planum Boreum, Viking and MOC images show low-albedo dune fields, including the vast Olympia Undae (unit d in Fig. 1), and others near the mouth of Chasma Boreale. These dunes appear to originate from a dark unit containing uneven bedding that forms the base of Planum Boreum and has been interpreted as a sand sea deposit [12]. Geologic mapping of this Boreum unit indicates that it approaches 1000 m in thickness west of Chasma Boreale, was emplaced during the Early Amazonian, and was extensively eroded prior to emplacement of north polar layered deposits that bury much of the unit [13]. The original volume of the dark Boreum unit may have approached that of Planum Boreum, or ~10^6 km^3. If the Boreum unit consists of relatively unaltered andesite, this would suggest a highly eroded, andesite bedrock source. Maximum transport distances for basaltic sand grains on Mars based on models of abrasion and TES observations for saltating materials on Mars indicate maximum transport distances of a few hundred kilometers [8] (we also note that the dark ST1 dunes apparently derived from the ST1 Syrtis Major volcanic flows near Isidis Planitia have not produced a ST1 signature significantly beyond the occurrence of the flows).

The only major source of sand in the vicinity of Planum Boreum is the VBF and associated materials of the Scandia region (unit vb). The VBF materials are generally thought to be clastic sediments derived from catastrophic fluvial erosion of martian highland rocks, (unit f), perhaps emplaced within a temporary, plains-filling ocean [14-15]. Structures within the VBF and Scandia region, including polygonal troughs, pitted and pancake domes, terraces, and depressions, suggest reworking of the VBF materials by near-surface, volatile-driven processes [13]. Because the highland materials have a ST1 TES signature, it would appear that the Boreum unit's ST2 signature must originate by alteration of ST1 rocks, which is consistent with the apparent water-associated emplacement and reworking history of the VBF. The VBF also may likely be the

source of most of the ST2 material throught the northern plains (Fig. 1), because the limited eolian transport distances noted previously preclude an origin from potential dust-covered ST2 highland and volcanic rocks (units h and v) in surrounding terrains.

Early Amazonian volcanic outcrops with ST2 signatures in and near the northern plains include rugged flows in northern Amazonis Planitia that originated near Olympus Mons (unit fr in Fig. 1) and dissected flow deposits in central and eastern Utopia Planitia originating from the Elysium rise thought to be lahars [13,16]. Some have argued that the pitted cones that occur along the margins of the VBF may be silicate volcanoes [e.g., 17], but their geologic associations seem to be more consistent with a sedimentary volcanic origin [13]. In any case, these materials all could have interacted significantly with water during their formation, resulting in weathered basaltic material. Alternatively, the ST2 signatures could result from saltation of VBF fines onto the outcrops or from an original andesite composition for the material.

Origin of the ST2 spectra. The ST2 unit displays the highest concentrations in the northern lowlands regions of Acidalia Planitia and the circumpolar sand seas [1]. Alteration rinds or coatings (i.e., sheet silicates, palagonites, and zeolite) are probably too fragile to resist much eolian abrasion. Silica coatings, however, may be sufficiently resistant to mechanical weathering to survive as coatings or cementing agents that can account for the ST2 spectral shape. Recent work by [18 and references therein] summarizes evidence for the probability of sedimentary silica existing on Mars and emphasizes the highly mobile nature of silica during near surface alteration of basaltic rocks under a wide variety of temperature, pressure, and fluid conditions. Palagonitization is a commonly proposed alteration process for the martian surface and the production of palagonites and secondary clays, both of which have been shown to be spectrally similar to high-silica volcanic glass, result in a high degree of silica mobilization [18 and references therein]. The geologic context of the VBF within a sedimentary basin with either transported or indigenous materials having interacted with surface or near-surface volatile-rich materials [13-14] supports an altered basalt classification for the TES ST2 unit in the northern lowlands.

References. [1] Bandfield J. L. et al. (2000) *Science*, 287, 1626-1630. [2] Hamilton et al. (2001) *JGR*, 106, 14733-14746. [3] Wyatt M. B. and McSween H. (2002) *Nature* 417, 263-266. [4] Christensen P. R. et al. (2000) *JGR*, 105, 9609-9622. [5] Bandfield J. L. et al. (2000) *JGR*, 105, 9573-9587. [6] Smith M. D. et al. (2000) *JGR*, 105, 9589-9609. [7] Bandfield J. L. (2002) *JGR* 107 (E6), 10.1029/2001JE00151. [8] Rogers D. and Christensen P. R. (2003) *JGR*, 108, 10.1029/2002JE001913. [9] Christensen P. R. et al. (2000) *JGR*, 105, 9632-9642. [10] Hamilton V. E. et al. (2002) *LPSC XXXIII*, Abs #1937. [11] Christensen P. R. (2003) *Nature*, 422, 45-48. [12] Byrne S. and Murray B.C. (2002) *JGR* 107, 10.1029/2001JE001615. [13] Tanaka K. L. et al. (2003) *JGR* 108, 10.1029/2002JE001908. [14] Parker T.J. et al. (1989) *Icarus*, 82, 111-145. [15] Baker V. R. et al. (1991) *Nature,* 352, 589-599. [16] Christiansen E. H. (1989) *Geology,* 17, 203-206. [17] Frey H.V. and Jarosewich M. (1982) *JGR,* 87, 9867-9879. [18] McLennan S. M. (2003) *Geology,* 31, 315-318.

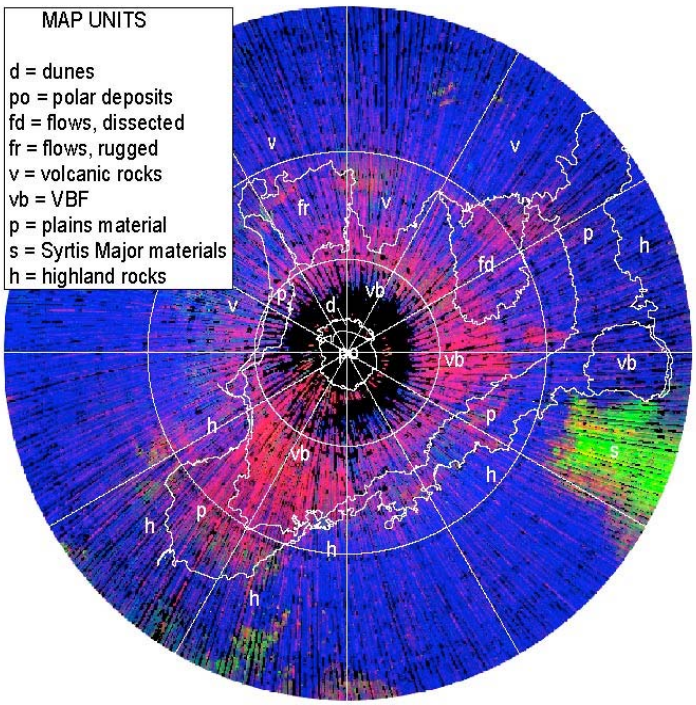

Figure 1. MGS-TES composition map of the northern hemisphere of Mars showing surfaces dominated by ST1 (green; basaltic spectra), ST2 (red, andesitic/weathered basalt spectra), and dust (blue). White lines outline geologic units described in text and generalized from [13].

OBSERVATIONS OF THE SEASONAL POLAR ICECAPS OF MARS AT 1064 nm.
Maria T. Zuber[1] and David E. Smith[2], [1]Dept of Earth Atmospheric and Planetary Sciences, Massachusetts Institute of Technology, 77 Massachusetts Ave. 54-918, Cambridge, MA 02139-4307, e-mail: zuber@mit.edu, [2]Laboratory for Terrestrial Physics, NASA Goddard Space Flight Center, Greenbelt, MD 20771, e-mail: David.E.Smith@nasa.gov.

Introduction. The Mars Orbiter Laser Altimeter (MOLA) [1, 2] is routinely making radiometric observations of Mars at a wavelength of 1064 nm. Although the altimeter function is no longer operational, the MOLA detector [3] continues to measure the reflectivity of the surface. Observations have been obtained almost continuously since the beginning of the Mars Global Surveyor (MGS) [4] mapping mission in February 1999, and are providing measurements relevant to understanding the seasonal cycling of CO_2 surface frost.

Radiometer Data. The field of view of the MOLA detector is approximately 800 μrad and from an altitude of 400 km receives reflected solar radiation from a roughly circular spot ~300 m in diameter. The data are acquired at a rate of 8 Hz and with a ground track velocity of the spacecraft of about 3 km s^{-1} the along-track resolution is slightly less than 400 m, thus providing an almost continuous profiling measurement of Martian surface brightness.

To determine reflectivity, the received optical power can be estimated by a mathematical model that utilizes the MOLA threshold setting and noise counts [5, 6]. Utilizing the link equation [7], observations are normalized to a constant mean solar flux assuming Lambertian scattering to yield a spectral radiance *(I/F)*.

For the purposes of this analysis the data were binned in 1 second time intervals representing a pixel size of 300 m x 3 km. The detector operates at 1064 ± 1 nm and measures the reflected signal strength to about 1%, and the receiver performance closely matches pre-launch testing. For the seasonal variations of interest in the present analysis the stability of the measurement is more important than the absolute calibration.

In this passive mode the radiometry is only obtainable when the surface of Mars is illuminated by sunlight. Further, since the orbit of the spacecraft is approximately sun-synchronous with a 2:00 PM local time the data are generally acquired under similar lighting conditions.

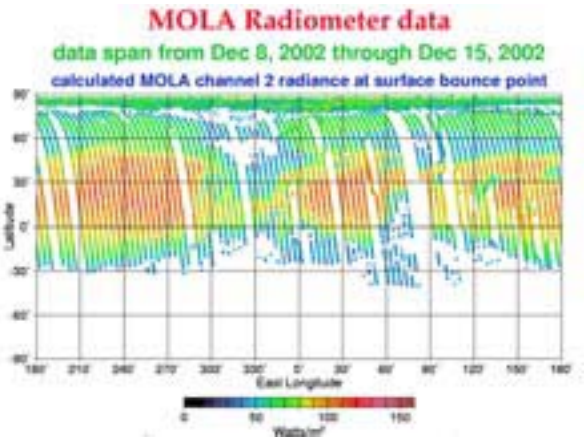

Fig. 1. *Uncalibrated passive radiometry observations acquired by MOLA between Dec 8 and 15, 2002. During the observation period the season was northern summer, with the sun illuminating the northern hemisphere of the planet. An example of the spacecraft being pointed off-nadir is evident in the figure at lat 25° N, 55° E. The spacecraft was traveling from south to north.*

However, the spacecraft instrument deck is not always pointed toward nadir and for much of the last year has been tilted off-nadir

by approximately 16^o in order to save on propellant used for attitude control. Further, the spacecraft is frequently rolled and pitched toward a particular target for camera observations, and the MOLA detector field of view follows the same path (Fig.1).

Seasonal Changes. The radiometry data show clear seasonal brightness changes in the polar regions that are a result of the deposition and sublimation of CO_2 on the surface at the onset of fall and in early spring. Fig. 2 shows the reflectivity at 1064 nm at the beginning of spring and early summer in the 2 hemispheres. Generally, the frost deposition in the north is distributed uniformly in longitude except on the polar cap itself, where the deposition and the sublimation appear to be related to the topography of the cap. In general areas that are less bright are lower in elevation and receive less solar illumination.

In the south the frost covering varies significantly with latitude and longitude (Fig. 2) and some regions appear even in early spring to have lost all their seasonal covering of CO_2. In contrast to the north polar region, the brightest regions do not correspond to those of highest elevation. The residual cap remains bright throughout the year and is probably a result of the exposure of water ice under the seasonal frost.

Seasonal frost on the southern polar residual cap is brighter than in the north and lasts longer in the spring. Both seasonal caps brighten as winter proceeds, and the brightness of both caps oscillates just before the frost sublimates back to the atmosphere, most markedly in the north. This phenomenon is observed in consecutive Martian years.

Observations of the process of frost deposition are more difficult to obtain due to most of the frost at high latitudes being deposited when the region is in darkness. However, the radiometry data do suggest that frost at the higher latitudes actually starts to form on the surface before the end of summer when the sun is approaching the equator but the pole is still illuminated. For the high northern latitudes this appears to begin around L_s= 150^o. The frost covering at both poles appears to have been similar, but not identical, in the two successive Mars years so far studied.

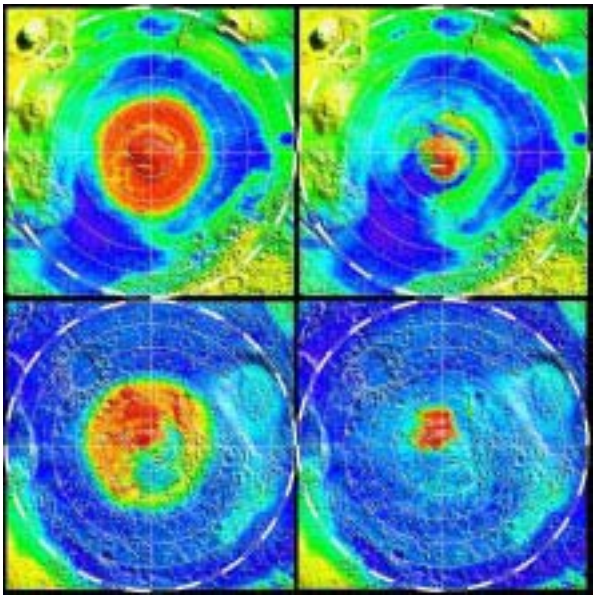

Fig. 2. *Seasonal images of the 1064-nm reflectance in the polar regions in early spring and early summer. The top 2 images are of the northern hemisphere (30^{o}N to pole) for L_s= 32^o (left) and L_s= 12^o (right). Bottom 2 images are of the southern hemisphere (30^o S to pole) for L_s= 212^o (left) and L_s= 272^o (right).*

References. [1] Zuber M.T. et al. (1992) *JGR, 97,* 7781-7797. [2] Smith D.E. et al. (2001) *JGR, 106,* 23,689-13,722. [3] Abshire J.B. et al. (2000) *Appl. Opt., 39, 90,* 2440-2460. [4] Albee A. et al. (2001) *JGR, 106,* 23,291-23,316. [5] Sun, X., et al. (1992) *IEEE Trans. Aero. Elec. Syst.,28,* 268-274. [6] Sun X. et al., (2001) *EOS Trans. Am. Geophys. Un.* [7] Gardner C.S. (1992) *IEEE Trans. on Geosci. Rem. Sens., 30,* 1061-1072.